Sink or Swim: A Tutorial on the Control of Floating Wind Turbines

Preprint

David Stockhouse,[1] Mandar Phadnis,[1] Aoife Henry,[1]
Nikhar Abbas,[1] Michael Sinner,[2] Manuel Pusch,[1,3]
and Lucy Pao[1,4]

1 University of Colorado Boulder
2 National Renewable Energy Laboratory
3 Munich University of Applied Sciences
4 Renewable and Sustainable Energy Institute

Presented at the 2023 American Control Conference (ACC)
San Diego, California
May 31 – June 2, 2023

See https://doi.org/10.23919/ACC55779.2023.10155920 for paper as published in proceedings.

NREL is a national laboratory of the U.S. Department of Energy
Office of Energy Efficiency & Renewable Energy
Operated by the Alliance for Sustainable Energy, LLC

Conference Paper
NREL/CP-5000-85082
August 2023

This report is available at no cost from the National Renewable Energy Laboratory (NREL) at www.nrel.gov/publications.

Contract No. DE-AC36-08GO28308

Sink or Swim: A Tutorial on the Control of Floating Wind Turbines

Preprint

David Stockhouse,[1] Mandar Phadnis,[1] Aoife Henry,[1] Nikhar Abbas,[1] Michael Sinner,[2] Manuel Pusch,[1,3] and Lucy Pao[1,4]

1 University of Colorado Boulder
2 National Renewable Energy Laboratory
3 Munich University of Applied Sciences
4 Renewable and Sustainable Energy Institute

Suggested Citation
Stockhouse, David, Mandar Phadnis, Aoife Henry, Nikhar Abbas, Michael Sinner, Manuel Pusch, and Lucy Pao. 2023. *Report Sink or Swim: A Tutorial on the Control of Floating Wind Turbines: Preprint*. Golden, CO: National Renewable Energy Laboratory. NREL/CP-5000-85082. https://www.nrel.gov/docs/fy23osti/85082.pdf.

NREL is a national laboratory of the U.S. Department of Energy
Office of Energy Efficiency & Renewable Energy
Operated by the Alliance for Sustainable Energy, LLC

This report is available at no cost from the National Renewable Energy Laboratory (NREL) at www.nrel.gov/publications.

Contract No. DE-AC36-08GO28308

Conference Paper
NREL/CP-5000-85082
August 2023

National Renewable Energy Laboratory
15013 Denver West Parkway
Golden, CO 80401
303-275-3000 • www.nrel.gov

NOTICE

This work was authored in part by the National Renewable Energy Laboratory, operated by Alliance for Sustainable Energy, LLC, for the U.S. Department of Energy (DOE) under Contract No. DE-AC36-08GO28308. Funding provided by the U.S. Department of Energy Office of Energy Efficiency and Renewable Energy Wind Energy Technologies Office. The views expressed herein do not necessarily represent the views of the DOE or the U.S. Government. The U.S. Government retains and the publisher, by accepting the article for publication, acknowledges that the U.S. Government retains a nonexclusive, paid-up, irrevocable, worldwide license to publish or reproduce the published form of this work, or allow others to do so, for U.S. Government purposes.

Cover Photos by Dennis Schroeder: (clockwise, left to right) NREL 51934, NREL 45897, NREL 42160, NREL 45891, NREL 48097, NREL 46526.

Sink or Swim: A Tutorial on the Control of Floating Wind Turbines

David Stockhouse[1], Mandar Phadnis[1], Aoife Henry[1], Nikhar Abbas[1], Michael Sinner[2], Manuel Pusch[1,3], and Lucy Y. Pao[1,4]

Abstract— **Within the rapidly growing wind energy sector, floating offshore wind turbines are expected to be the fastest growing portion. This is largely driven by the immense offshore wind resources that are mostly over deep water, where fixed-bottom concepts become cost-prohibitive. However, compared to fixed-bottom wind turbines, floating wind turbines are more dynamic and exhibit potential instabilities, which requires advanced control technologies to ensure a safe and efficient operation. Beyond their existing objectives of maximizing power production while minimizing structural loads, floating wind turbine controllers must also avoid large platform oscillations and accommodate ocean wave and current disturbances. This paper provides an overview of the challenges and opportunities in the control of floating offshore wind energy systems.**

I. Introduction

Climate change is a serious threat facing humanity. The United States (US) and many other countries are increasing the amount of electrical power generated from renewable energy sources in an effort to combat climate change and ensure energy independence. The US has set goals to achieve a 100% decarbonized electric grid by 2035 and a net-zero emissions economy by no later than 2050 [1]. Renewable energy currently accounts for about 20% of the US power grid. In the US in 2021, wind and solar photovoltaic generation supplied 9.1% [2] and 4% [3] of total electricity generation, respectively; and the latest publicly available data shows that hydropower represented 6.6% of all electricity generated in the US in 2019 [4]. As wind farms have been built in many of the best wind resource areas on land, the US and many other countries are turning to offshore wind for further growth of wind power capacity. The US has committed to deploy 30 GW of offshore wind by 2030 [5], a significant increase from the current 0.04 GW of installed offshore wind in the country [6]. Many other countries have also established ambitious goals or plans to increase the amount of installed offshore wind power [6, 7].

This work was authored in part by the National Renewable Energy Laboratory, operated by Alliance for Sustainable Energy, LLC, for the U.S. Department of Energy (DOE) under Contract No. DE-AC36-08GO28308. Funding provided by the U.S. Department of Energy Office of Energy Efficiency and Renewable Energy Wind Energy Technologies Office, and by a Palmer Endowed Chair at the University of Colorado Boulder. The views expressed in the article do not necessarily represent the views of the DOE or the U.S. Government. The U.S. Government retains and the publisher, by accepting the article for publication, acknowledges that the U.S. Government retains a nonexclusive, paid-up, irrevocable, worldwide license to publish or reproduce the published form of this work, or allow others to do so, for U.S. Government purposes.

[1] University of Colorado Boulder, Boulder, CO
[2] National Renewable Energy Laboratory, Golden, CO
[3] Munich University of Applied Sciences, Munich, Germany
[4] Renewable and Sustainable Energy Institute, Boulder, CO

The vast majority of existing offshore wind turbines are fixed-bottom turbines, where the turbine tower is fixed to the seafloor using a rigid substructure. However, the majority of offshore wind resources are over water depths greater than 60 meters [6, 8] (a cost-prohibitive depth for fixed-bottom turbines), and floating turbines are better suited to these regions. Floating wind turbines, however, remain in the developmental stage with costs still considerably higher than those of land-based or fixed-bottom offshore turbines, the floating platform being a significant cost driver.

Several platform designs have been explored for floating wind turbines [6, 8, 9]. Some of the initial platform designs have been borrowed and adapted from the oil and gas industry; these floating platforms tend to be very massive and expensive to manufacture. In order to drive down costs, lighter-weight platform designs such as the SpiderFLOAT [10] are being developed. Controller designs become even more critical with such lighter-weight platforms.

One floating offshore wind turbine (FOWT) challenge that has been a focus of a number of studies [11–16] is the platform fore-aft instability that can occur when trying to use a standard blade pitch controller developed for fixed-bottom wind turbines. When the FOWT tilts forward, the effective wind speed coming into the rotor plane increases. In above-rated wind conditions, this causes the blade-pitch controller to pitch the blades to let more wind go by to keep the rotor speed constant as typically desired. However, pitching the blades also decreases rotor thrust, causing the FOWT to tilt forward more, which can lead to instability. A symmetrical response happens when the FOWT tilts backward: as the effective wind speed decreases, the controller pitches the blades to catch more wind, and the rotor thrust then increases, which leads the FOWT to tilt backward more. Since FOWTs are excited by both wind and waves and have more degrees of freedom (DOFs) than fixed-bottom turbines, it is important to analyze the dynamic coupling between the floating platform and the wind turbine. The development of multi-input, multi-output (MIMO) controllers can mitigate the coupling [17] and also allows for accommodating advanced actuation concepts of the floating platform [18–21].

By combining multiple FOWTs into a wind farm, additional challenges and opportunities arise. The control of land-based and fixed-bottom wind farms is already a very active research area [22–28]. It has been shown via field tests on commercial wind farms that increases of more than 1% in energy production can be achieved through coordinated control of wind turbines to account for wake interactions. For a hundred-megawatt-scale wind farm, a few percent increase in power production over a year would yield millions of dollars in additional revenue. Since FOWTs are newer, the understanding and modeling of their wake characteristics is still in development. However, initial studies indicate that the wakes behind FOWTs may dissipate faster compared to wakes behind fixed-bottom wind turbines [29, 30]. This suggests a potential advantage of floating offshore wind farms: Since utility-scale fixed-bottom wind farms can lose 10–20% of their energy production per year due to wake interactions between turbines [31], for the same layout as a fixed-bottom wind farm in similar wind conditions, a floating wind farm may be able to produce significantly more energy by naturally mitigating wake interactions.

In this article, the focus is on control of horizontal-axis wind turbines (HAWTs), as they have been dominant among land-based and fixed-bottom offshore wind turbines. Section II reviews the basic controllers for land-based and fixed-bottom HAWTs. Then, several fundamental control approaches for FOWTs are outlined in Section III, including overviews of floating platform configurations and floating wind turbine dynamics. Advanced control methods that have been explored for FOWTs are discussed in Section IV. Emerging opportunities that floating wind farms may provide are enumerated in Section V. Section VI overviews the state-of-the-art software codes and design tools that are currently available, and also reviews a few experimental FOWT validation campaigns. In Section VII, we point out a couple other floating wind turbine configurations that are being explored beyond HAWTs. Finally, Section VIII provides an outlook for floating wind energy.

II. Fixed-Bottom Wind Turbine Control Basics

Important aspects of conventional wind turbine control are examined here before considering the impact that the floating environment has on the control design. A detailed tutorial on the control of land-based wind turbines is provided in [32].

A. Power Flow

The key goal of wind turbine control is to regulate the extraction of power from the wind into the electrical grid. Slender aerofoils—the blades—are mounted radially to a central hub making up the wind turbine rotor. The spinning rotor acts as a store of rotational kinetic energy, exchanging power with the inflowing wind and a connected electrical generator. The total aerodynamic power available in the wind, P_{inflow}, grows with the cube of the wind speed v normal to the rotor plane:

$$P_{\text{inflow}} = \frac{1}{2}\rho\pi R^2 v^3, \tag{1}$$

where ρ is the air density and R is the blade length. The power flowing from the wind into the rotor is

$$P_{\text{rot}} = C_p(\lambda, \beta) P_{\text{inflow}}, \tag{2}$$

mediated by the power coefficient $C_p(\lambda, \beta)$ dependent on the blade pitch angle β and tip-speed ratio (TSR) $\lambda = \frac{R\Omega_{\text{rot}}}{v}$, with Ω_{rot} the rotational speed of the rotor. C_p is upper-bounded by the Betz limit, 0.593 [33], and practical aerodynamic inefficiencies limit this value further.

The rotational energy is transferred to an electrical generator through a drivetrain and extracted into the grid as electricity. The rotational speed Ω_{rot} is typically less than 1 Hz (60 RPM), which is an inefficient speed for electrical power conversion [33]. Hence, many designs use a gearbox in the drivetrain to step-up the rotational speed of the rotor (low-speed shaft) into the generator (high-speed shaft). The rotational speed of the generator shaft is $\Omega_{\text{gen}} = N_{\text{gb}}\Omega_{\text{rot}}$, where N_{gb} is the gearbox ratio (in a direct-drive generator, $N_{\text{gb}} = 1$). Power is extracted by the generator with efficiency $\eta_{\text{gen}} < 1$ by exerting a controllable resistance torque τ_{gen} on the rotating system, yielding the power P_{gen} transmitted to the grid:

$$P_{\text{gen}} = \eta_{\text{gen}}\tau_{\text{gen}}\Omega_{\text{gen}}. \tag{3}$$

For simplicity, we assume here $\eta_{\text{gen}} \approx 1$ and ignore the impact of generator inefficiency. An imbalance between the power flowing into the rotor and out of the generator causes a change in the stored kinetic energy (i.e., rotor acceleration), leading to the below dynamics (4). The rotor combined with the drivetrain and generator (housed in the nacelle) is called the rotor-nacelle assembly (RNA), which sits on top of the tower with controllable yaw direction. In this section, the yaw is assumed to be constant and aligned with the inflow wind direction. In Section V, yaw control is discussed in the context of wind-wake interactions between inflow-aligned turbines in a wind farm.

B. Wind Turbine Dynamics

The dynamics of a wind turbine can be represented in a simplified form as [32]

$$\frac{J_{\text{rot}}}{N_{\text{gb}}}\dot{\Omega}_{\text{gen}} = \left(T_{\text{aero}}\left(\Omega_{\text{gen}}, v, \beta\right) - N_{\text{gb}}\tau_{\text{gen}}\right), \tag{4}$$

where J_{rot} is the rotational inertia of the rotor-drivetrain-generator system. The aerodynamic torque $T_{\text{aero}}\left(\Omega_{\text{gen}}, v, \beta\right)$ is a nonlinear function related to the aerodynamic power as $T_{\text{aero}} = \frac{P_{\text{rot}}}{\Omega_{\text{rot}}}$. At steady-state equilibrium, the power flow is balanced and $T_{\text{aero}} = N_{\text{gb}}\tau_{\text{gen}}$. We can linearize the dynamics (4) around an equilibrium point:

$$\begin{aligned}\dot{\tilde{\Omega}} - \frac{N_{\text{gb}}}{J_{\text{rot}}}\frac{\partial T_{\text{aero}}}{\partial \Omega}\tilde{\Omega} &= \frac{N_{\text{gb}}}{J_{\text{rot}}}\left(\frac{\partial T_{\text{aero}}}{\partial v}\tilde{v} + \frac{\partial T_{\text{aero}}}{\partial \beta}\tilde{\beta} - N_{\text{gb}}\tilde{\tau}\right) \\ \tilde{P} &= \overline{\tau}\tilde{\Omega} + \overline{\Omega}\tilde{\tau},\end{aligned} \tag{5}$$

where the notation $\tilde{\times}$ represents a perturbation from equilibrium $\overline{\times}$, so $\times = \overline{\times} + \tilde{\times}$. Some subscripts have been dropped for brevity. The aerodynamic sensitivity gradients $\frac{\partial T_{\text{aero}}}{\partial \times}$ are estimated from a nonlinear model at the equilibrium operating point (shown in Fig. 2).

C. Baseline Control - Overview

In low to medium wind speeds ($\overline{v} < v_{\text{rated}}$), the goal for wind turbine operation is to maximize power production (i.e., maximize the power coefficient $C_p(\lambda, \beta)$). The maximum power coefficient $C_{p,\text{opt}}$ is generally attained at a

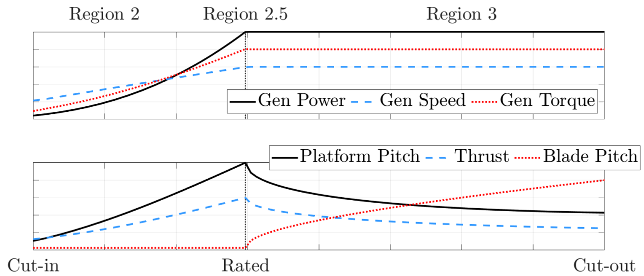

Fig. 1. Operating regions for a variable-speed pitch-actuated wind turbine. The axes are non-dimensionalized. Region 2 is below-rated (variable-speed) operation, where the goal is to maximize power production. Region 3 is above-rated (constant-speed) operation, where the generator is at rated equilibrium and the blades are pitched to regulate power output, consequently influencing aerodynamic thrust and the platform dynamics.

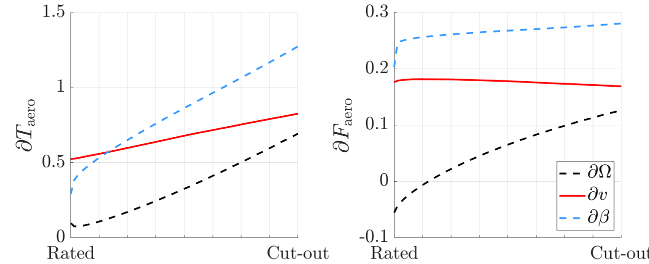

Fig. 2. Aerodynamic torque T_{aero} and thrust F_{aero} sensitivities in response to change in generator speed $\partial\Omega$, wind speed ∂v, and blade pitch $\partial\beta$. Each curve is non-dimensionalized to represent the relative strength of each sensitivity compared to the size of typical signals. The dashed lines for $\partial\Omega$ and $\partial\beta$ are multiplied by -1 to provide (negative) comparison against ∂v.

certain TSR λ_{opt} and so-called "fine" blade pitch β_{fine}. The rotor speed is regulated to keep the TSR at the optimal value $\lambda = \lambda_{\text{opt}}$ in varying wind speeds while blade pitch is constant $\beta = \beta_{\text{fine}}$. Standard control approaches for below-rated ("Region-2") operation are based on feeding back generator speed Ω_{gen} to control the generator torque τ_{gen} [32, 34].

Once the wind speed is high enough ($\overline{v} > v_{\text{rated}}$), the generator reaches its rated electrical loading capacity and the mode of operation of the turbine switches to one of generating a fixed power $P_{\text{rated}} = \tau_{\text{rated}}\Omega_{\text{rated}}$. Most above-rated ("Region-3") controllers hold constant torque $\tau_{\text{gen}} = \tau_{\text{rated}}$ and use blade-pitch β feedback to keep generator speed Ω_{gen} near its rated value Ω_{rated}. Additional objectives include the reduction of structural loads, the protection of the individual hardware components, and a high power quality, with design-specific order of priority.

In Fig. 1, the steady-state relationship between relevant input and output variables is depicted for the two described operating regions, where "Rated" denotes the wind speed v_{rated} dividing below- and above-rated operation. The transition between the two regions generally leads to nonlinear behavior, which is often smoothed by implementing advanced switching logic or specific transition-region ("Region-2.5") control laws [35, 36].

Below-rated control approaches developed for fixed-bottom offshore or land-based wind turbines can be generally applied to FOWTs without the need of significant modification. Hence, below-rated control is not discussed in detail here and the reader is referred to references like [34, 36]. For above-rated control, however, coupling of the wind turbine dynamics with the floating platform dynamics can be critical and generally require a modification or redesign of existing control laws. These are reviewed in the next section.

D. Baseline Control - Above-Rated Control Approaches

The most common above-rated baseline control law is a proportional-integral (PI) or proportional-integral-derivative (PID) controller designed for the linearized dynamics (5) that uses blade pitch $\tilde{\beta}$ to regulate generator speed error $\tilde{\Omega}$ to zero [32]. Note that if generator torque τ_{gen} is held constant ($\tilde{\tau} = 0$), variations in generator speed $\tilde{\Omega}$ are passed directly on to power $\tilde{P}$, so regulating speed and power are equivalent for a single-loop controller (there is a nontrivial difference when combined with an auxiliary generator-torque feedback loop—see Section III-F).

The aerodynamic sensitivities in (5) vary significantly across operating points (see Fig. 2). To maintain consistent closed-loop transient behavior using a linear controller, the controller gains are typically scheduled at each operating point and adjusted during operation as the wind speed $\overline{v}$ varies [32]. Because of the monotonic relationship between steady wind $\overline{v}$ and steady blade pitch $\overline{\beta}$ (see the above-rated portion of Fig. 1), the scheduling parameter can be an estimate of steady-state wind speed or blade pitch, and the latter is often used for its simplicity [33, 36].

The baseline PI controller is

$$\tilde{\beta} = k_p \left(\tilde{\Omega} - \tilde{\Omega}_{\text{ref}}\right) + k_i \int \left(\tilde{\Omega} - \tilde{\Omega}_{\text{ref}}\right) dt \qquad (6)$$

where k_p and k_i are proportional and integral gains, respectively. A zero reference $\tilde{\Omega}_{\text{ref}} = 0$ (i.e. rated operation) is assumed for most controllers, except for a handful of advanced control approaches [37, 38]. The closed-loop system is modeled by a second-order differential equation

$$0 = \dot{\tilde{\Omega}} + 2\zeta_{\text{PI}}\omega_{\text{PI}}\tilde{\Omega} + \omega_{\text{PI}}^2 \int \tilde{\Omega} dt, \qquad (7)$$

where

$$\omega_{\text{PI}} = \sqrt{-k_i \frac{N_{\text{gb}}}{J_{\text{rot}}} \frac{\partial T_{\text{aero}}}{\partial \beta}} \qquad (8)$$

$$\zeta_{\text{PI}} = -\frac{1}{2\omega_{\text{PI}}} \frac{N_{\text{gb}}}{J_{\text{rot}}} \left(\frac{\partial T_{\text{aero}}}{\partial \Omega} + \frac{\partial T_{\text{aero}}}{\partial \beta} k_p \right). \qquad (9)$$

From (8) and (9), the controller gains k_p and k_i can be analytically derived given a desired natural frequency ω_{PI} and damping ratio ζ_{PI} [36, 39]. We can then design closed-loop dynamics to be consistent over a large wind speed range and compute PI gain schedules to satisfy the desired behavior. Tuning ζ_{PI} and ω_{PI} instead of k_p and k_i is generally more intuitive, where ω_{PI} allows for directly balancing disturbance rejection bandwidth and actuator usage.

In some designs, variations of generator power may be more detrimental than those of generator speed. A common secondary control loop for land-based systems attempts to prevent power fluctuations $\tilde{P}$ from being caused by speed fluctuations $\tilde{\Omega}$ by actuating generator torque inversely with speed, $\tau_{\text{gen}} = \frac{P_{\text{rated}}}{\Omega_{\text{gen}}}$. This so-called constant-power control law typically leads to increased variations in generator speed while improving power quality. Details on corresponding control laws can be found in [17, 36].

III. FOWT Control Fundamentals

In this section, we first discuss some practical aero-hydro-structural engineering challenges in FOWT design, and then turn to control approaches that build on the fixed-bottom baseline controller.

A. The Floating Environment

Early work in system design for floating wind turbines was inspired by pre-existing offshore oil and gas rigs. The realization that some fundamentally different requirements govern floating wind plants quickly showed that floaters optimized for a wind turbine application could reduce costs more than trying to adapt previous work from another field, despite a few technological hurdles [40].

A FOWT's operating environment is certainly more hostile than that of its land-based and fixed-bottom counterparts. Over long timescales (years), corrosive seawater and repeated wave impacts cause erosion and fatigue of substructure components, necessitating maintenance and replacement. Over shorter timescales (seconds), underdamped platform motion and irregular wave forces cause a dynamic disturbance on the FOWT, resulting in additional component fatigue and reduced grid power quality. Solving these challenges in a cost-competitive manner requires innovative approaches in turbine, platform, and controller design [41].

B. Floating Platform Types

A FOWT sits atop a platform which must provide stability from tipping in the presence of wind and wave forces while withstanding loading on its own substructure. An overview of common FOWT platform substructures (pictured in Fig. 3) is briefly given here, and other authors have previously examined the topic in more depth [9, 40, 42].

Barge platforms have been adapted from their success in other maritime domains including oil and gas extraction, where they achieve stability from their large areas spread over the sea surface [9]. While the large exposed surface area of a barge is advantageous for human-centric operations such as fully-staffed oil and gas rigs [40], different objectives govern FOWT operation, so barges have been all but replaced with FOWT-oriented platforms in recent project designs [6].

Spar-buoy platforms consist of a massive central rod extending from sea level down to approximately the same extent under the sea as the tower reaches above the sea surface [9]. The spar acts as a counterbalance against the weight of the turbine and tower, providing stability and damping, but requiring significant material to manufacture.

Semisubmersible platforms attain stability from buoyant elements spread over a wide lateral area like a barge but keep most of the substructure submerged to avoid the high wave energy at the sea surface.

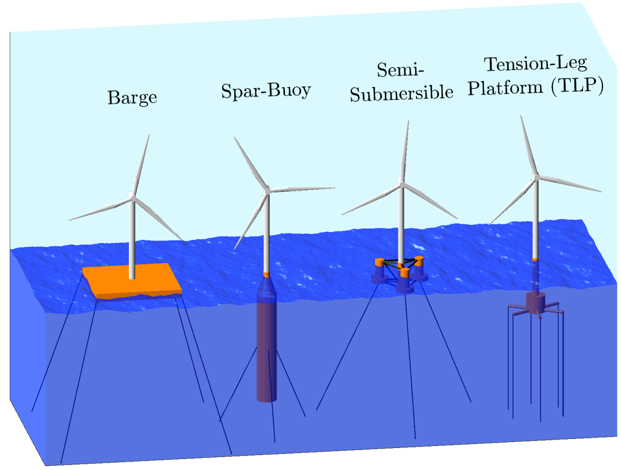

Fig. 3. Depiction of four platform types discussed in Section III-B with a mounted DTU 10 MW reference wind turbine [43]. The example barge, spar-buoy, and TLP are based on the case studies in [9], and the semi-submersible is based on the OC4-DeepCwind platform [44].

These platform types typically use catenary or semi-taut mooring lines attached to anchors on the seafloor to keep the platform position close to its installed location. However, such mooring configurations still allow some variation in lateral platform position during operation, depending on the dominant wind direction and control strategy.

In contrast, *tension-leg platforms* (TLPs) rely on balancing excess platform buoyancy with nearly vertical taut mooring lines to keep platform displacements small. The wind-loaded stiffness allows for imbalanced cable tensions, and snap-tension loads of significant force pose a risk of catastrophic failure. While the TLP has been studied in simulations and some lab experiments, the technology has yet to be validated at utility scale.

Regardless of platform type and mooring configuration, some platform motion will be transferred to the RNA to couple with generator dynamics. While a source of disturbance, this coupling grants the turbine controller considerable authority over platform fore-aft motion.

C. Floating Wind Turbine Dynamics

The main challenge in controlling a FOWT is the fore-aft motion of the RNA at the top of the tower. Fixed-bottom turbines experience some RNA motion due to tower flexibility that can be excited by the blade pitch controller, but the range of motion is limited by the deflection of the tower [45]. In a FOWT, platform surge translation x_{ptfm} and pitch rotation ϕ_{ptfm} (both fore-aft motions—see Fig. 4) are transferred to the RNA through the tower (whose flexible deflections are negligible compared to the rigid motion of the platform):

$$\begin{aligned} x_{\text{RNA}} &= x_{\text{ptfm}} + H_t \sin\phi_{\text{ptfm}} \approx H_t \phi_{\text{ptfm}} \\ \phi_{\text{RNA}} &= \phi_{\text{ptfm}} + \phi_{\text{shaft}}, \end{aligned} \tag{10}$$

where x_{RNA} and ϕ_{RNA} are the fore-aft translational (surge) and rotational (pitch) deflections of the RNA, respectively, H_t is the distance between the RNA and axis of rotation ($\approx$ tower height), and ϕ_{shaft} is the shaft tilt angle (see Fig. 10).

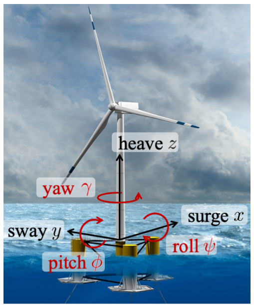

Fig. 4. Six degree-of-freedom representation of a FOWT platform. Black arrows indicate translational degrees of freedom and red arrows indicate rotational degrees of freedom. Original image created by Josh Bauer, NREL.

If the translational stiffness due to mooring forces on the wind-loaded FOWT system is high, then x_{ptfm} stays near its steady-state settling position and the FOWT RNA motion is captured using a single degree of freedom for platform pitch (some designs instead account for the surge DOF and neglect pitch, such as when using a tension-leg platform [46]). The small-angle approximation holds for modeling platform pitch rotation in typical operation.

Both RNA fore-aft velocity and tilt deflection affect FOWT power extraction by changing the magnitude and direction of the wind speed vector from the inflow velocity v_{inflow}. The RNA velocity $\dot{x}_{\text{RNA}}$ adds to v_{inflow} and the tilt offset ϕ_{RNA} requires a projection normal to the rotor plane:

$$v = v_{\text{inflow}} \cos \phi_{\text{RNA}} - \dot{x}_{\text{RNA}} \approx v_{\text{inflow}} - H_t \dot{\phi}_{\text{ptfm}}. \qquad (11)$$

In below-rated winds, this rotor-relative wind vector (nonlinear form) affects mean power as a cubic in (1). The tilt offset and fore-aft velocity compete in their effects on mean power production [47]. A simplified model of the power available to a FOWT with static and dynamic platform pitch activity is shown in Fig. 5. Because much of the dynamic platform motion occurs in response to higher-frequency wind speed variations, accurately describing the impact of the dynamic motion on power output requires dynamics that are neglected in this static model, and the benefits expected from dynamic motion are difficult to realize in a higher-order system model [47]. Power losses due to mean platform tilt are confirmed by higher-order simulations, and by actuating the platform to tilt forward (compensating the shaft tilt), there is the potential for a Region-2 platform controller to boost mean power beyond that of a fixed-bottom turbine.

Above rated, where blade pitch is used to regulate power, the relative wind speed induced by the platform (11) (with small-angle approximation) causes dynamic coupling between the generator and platform and acts as a disturbance on the primary control loop (6). The platform pitch DOF ϕ_{ptfm} is modeled simplistically as a damped rotational spring:

$$J_\phi \ddot{\phi}_{\text{ptfm}} + D_\phi \dot{\phi}_{\text{ptfm}} + K_\phi \phi_{\text{ptfm}} = H_t F_{\text{aero}} \left(\Omega_{\text{gen}}, v, \beta \right), \qquad (12)$$

where J_ϕ is the total rotational inertia about the platform pitch axis, D_ϕ is the hydrodynamic damping, and K_ϕ is the hydrostatic stiffness (a combination of buoyancy, mooring, and gravitation forces). The parameters J_ϕ, D_ϕ, and K_ϕ can be identified from a nonlinear model using numerical

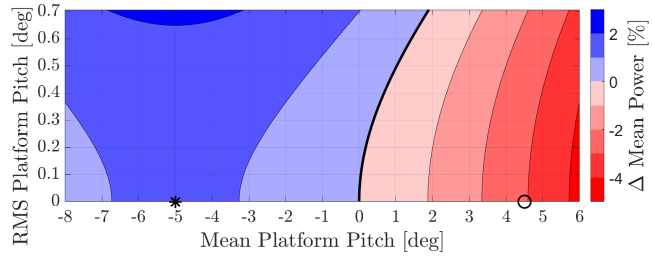

Fig. 5. Fractional difference in mean power available to a FOWT at a below-rated wind speed relative to the same turbine with constant zero platform pitch (fixed-bottom). This analysis uses a static power model averaging over FOWT relative wind velocity, (1) combined with (11). The relative wind vector is generated by an ideal FOWT undergoing undamped sinusoidal platform pitch oscillations of a given RMS amplitude (y-axis) at a frequency of 0.06 Hz combined with a mean offset (x-axis). Rotor-shaft tilt is $\phi_{\text{tilt}} = +5^\circ$ (see Fig. 10). Dynamic motion increases the available power because of the biased mean resulting from the cube of a mean-offset sinusoid. Due to FOWT dynamics, power gains from dynamic motion are difficult to realize, but power losses due to mean platform pitch are well-known. $\circ$ indicates the mean platform pitch for USFLOWT [21], and $*$ indicates the optimal mean platform pitch $\phi_{\text{ptfm}} = -\phi_{\text{shaft}}$.

linearization or through system identification [48]. F_{aero} is the aerodynamic thrust force on the rotor (similar to T_{aero} in (4)), which generates a pitching moment on the platform through the lever-arm H_t of the tower. For the purpose of control design, (12) is linearized about a steady-state platform pitch $\overline{\phi} \approx 0$ with the turbine in the rated equilibrium ($\overline{\Omega} = \Omega_{\text{rated}}$ and $\overline{\tau} = \tau_{\text{rated}}$):

$$\begin{aligned} J_\phi \ddot{\tilde{\phi}} + D_\phi \dot{\tilde{\phi}} + K_\phi \tilde{\phi} \\ = H_t \left(\frac{\partial F_{\text{aero}}}{\partial \Omega} \tilde{\Omega} + \frac{\partial F_{\text{aero}}}{\partial v} \tilde{v} + \frac{\partial F_{\text{aero}}}{\partial \beta} \tilde{\beta} \right), \end{aligned} \qquad (13)$$

where the thrust force sensitivities $\frac{\partial F_{\text{aero}}}{\partial \times}$ are calculated in the same way as the torque T_{aero} sensitivities in (5). Example values of the torque and thrust sensitivities for the DTU 10 MW reference wind turbine [43] are compared in Fig. 2.

Beyond the rotor's effect on the platform pitch through F_{aero}, the platform motion further influences the dynamics through the linearized relative wind speed (11), which is substituted into the disturbance perturbation $\tilde{v}$ in (5) and (13): $\tilde{v} = -H_t \dot{\tilde{\phi}}$. The coupled dynamics form a third-order system, which is represented in state-space with state $\boldsymbol{x} = \begin{bmatrix} \tilde{\Omega} & \tilde{\phi} & \dot{\tilde{\phi}} \end{bmatrix}^\top$ and control input $\boldsymbol{u} = \begin{bmatrix} \tilde{\beta} & \tilde{\tau} \end{bmatrix}^\top$ as $\dot{\boldsymbol{x}} = \boldsymbol{A}\boldsymbol{x} + \boldsymbol{B}\boldsymbol{u}$:

$$\dot{\boldsymbol{x}} = \left[\begin{array}{c|cc} A^\Omega & 0 & A^\Omega_\phi \\ \hline 0 & 0 & 1 \\ A^\phi_\Omega & A^\phi_K & A^\phi_D \end{array} \right] \boldsymbol{x} + \left[\begin{array}{cc} B^\Omega_\beta & B^\Omega_\tau \\ \hline 0 & 0 \\ B^\phi_\beta & 0 \end{array} \right] \boldsymbol{u}, \qquad (14)$$

where the individual matrix elements are given in the Appendix. The block form of the system matrix $\boldsymbol{A}$ and input matrix $\boldsymbol{B}$ indicates the separation into generator (5) and platform (13) dynamics. The off-diagonal blocks A^Ω_ϕ and A^ϕ_Ω represent coupling between the two DOFs. The outputs $\boldsymbol{y} = \boldsymbol{C}\boldsymbol{x} + \boldsymbol{D}\boldsymbol{u}$ can be chosen based on the available system measurements used for control feedback, typically a subset of the states in $\boldsymbol{x}$ or generator power $\tilde{P}$ [17]. Note that under the common definitions of the inputs β and τ,

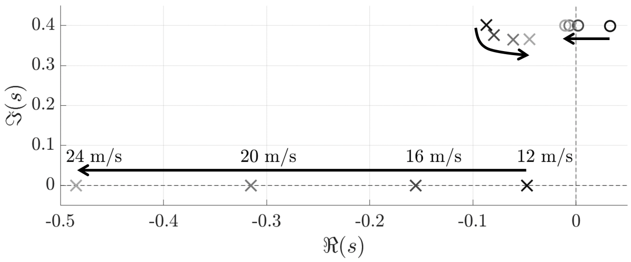

Fig. 6. Pole-zero plot of the 2-DOF FOWT transfer function from blade pitch $\tilde{\beta}$ to generator speed $\tilde{\Omega}$ (equivalently, generator power $\tilde{P}$) across Region-3 operating points using USFLOWT model parameters. $\times$ markers denote poles and $\circ$ markers denote zeros. Darker markers denote operating points near rated while lighter markers are near cut-out, and arrows indicate the movement of poles and zeros with increasing wind speed.

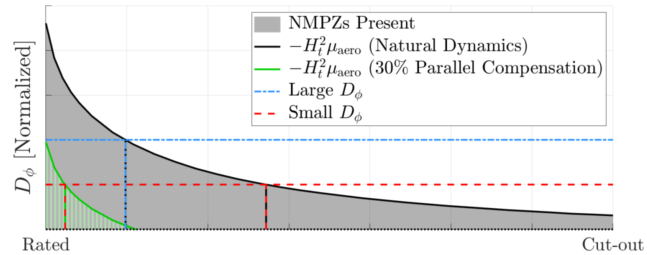

Fig. 7. Comparison of the left-hand side of (15) with different platform damping coefficients D_ϕ for the DTU 10 MW reference wind turbine [43]. Tracing a line of constant D_ϕ, the wind speeds over which the line overlaps with the shaded region admit NMPZs. The green curve shows the same quantity after parallel compensation has been applied to the system, tuned to 30% of the full platform-compensating gain (Section III-F.2).

the components of $\boldsymbol{B}$ are all negative, implying an inverted input response (i.e., an *increase* in either input will generally lead to a *decrease* in associated steady-state outputs).

D. Non-Minimum Phase Zeros and Closed-Loop Instability

We now turn from state-space to the transfer function representation of the system from $\tilde{\beta}$ to $\tilde{\Omega}$, which is regulated by the traditional wind turbine blade-pitch controller. The poles and zeros of this transfer function $G_{\beta}^{\Omega}(s)$ are plotted in Fig. 6, showing their evolution across Region-3 operating points. In closing the loop with a negative feedback controller, the root locus leads from the underdamped platform pitch poles toward the open-loop zeros (which are typically in the direction of the positive real axis of the s-plane), so the feedback reduces the platform damping ratio. Near rated, the transfer function may have zeros in the right half-plane (RHP), also called non-minimum phase zeros (NMPZs), which will make the linearized system unstable if the gain is high enough to draw the poles into the RHP (often called "negative damping" [11, 12] due to the damping ratio of two system poles reducing below zero). Applying the unmodified baseline fixed-bottom controller to a nonminimum-phase system may trigger this instability. Fischer et al. [14] show that the rational transfer function $G_{\beta}^{\Omega}(s)$ has NMPZs if the following condition holds:

$$-H_t^2\mu_{\text{aero}} > D_\phi, \tag{15}$$
$$\text{where } \mu_{\text{aero}} = \frac{\partial F_{\text{aero}}}{\partial v} - \frac{\partial T_{\text{aero}}}{\partial v}\frac{\partial F_{\text{aero}}/\partial \beta}{\partial T_{\text{aero}}/\partial \beta}.$$

Inequality (15) is plotted over Region-3 wind speeds in Fig. 7 using the DTU 10 MW reference wind turbine [43] parameter values compared to two choices of platform damping D_ϕ.

The presence of poles in the RHP means that the closed-loop linearized system (14) is unstable in a bounded-input bounded-output (BIBO) sense. This implies that the rated equilibrium point of the nonlinear dynamics is unstable in the sense of Lyapunov [49], however, in the nonlinear dynamics (4) and (12) this instability is only local. State trajectories initially perturbed from equilibrium do not diverge unbounded but rather asymptotically approach a stable periodic orbit in the state space, shown by the black curve in Figs. 8 and 9. The FOWT literature generally only considers stability of the equilibrium point, while the steady-state oscillations of the limit cycle are regarded as unstable behavior. In turbulent wind (red curve), transient disturbances across a wide range of frequencies lead to aperiodic behavior, but the system still incurs significant oscillatory motion about the unstable equilibrium, causing structural loading and poor power quality. FOWT controller designs generally aim to maintain linearized stability at all operating points to avoid this performance degradation. Several modifications have been proposed in the literature to maintain closed-loop stability using existing sensors, actuators, and control design approaches (see also Section IV).

E. Controller Detuning

Stability can be maintained in the presence of NMPZs by reducing the feedback gain, or detuning [11] (shown by the blue curve in Figs. 8 and 9). Using the PI controller parameterization from Section II-D, it is common to detune the closed-loop natural frequency ω_{PI} to be below the frequency of the NMPZs, which is approximately equal to the resonant frequency of the platform, ω_{ptfm} [12]. However, this method is imprecise, as a global detuning approach sacrifices control bandwidths at higher wind speeds and may still destabilize the closed-loop system if natural damping is low.

A more precise approach is to schedule the detuning at each operating point based on the analytical stability of the linearized system [16, 50, 51]. Using a stability margin based on the closed-loop sensitivity function [52] offers stability robustness in the presence of inaccurate modeling, neglected dynamics, or scheduling parameter uncertainty. Under such an ad hoc detuning schedule, the transient behavior is no longer held consistent over the operating region, but the ability to satisfy distinct objectives at differing wind speeds justifies a somewhat variable transient response.

F. Multi-Loop FOWT Control

Detuning requires a compromise in performance at near-rated wind speeds. In reducing the closed-loop bandwidth to achieve stability, the controller becomes less aggressive in rejecting disturbances and regulating power [21]. Adding auxiliary feedback loops to the baseline controller (the primary control loop) allows us to tune a stable response without a significant increase to controller complexity or

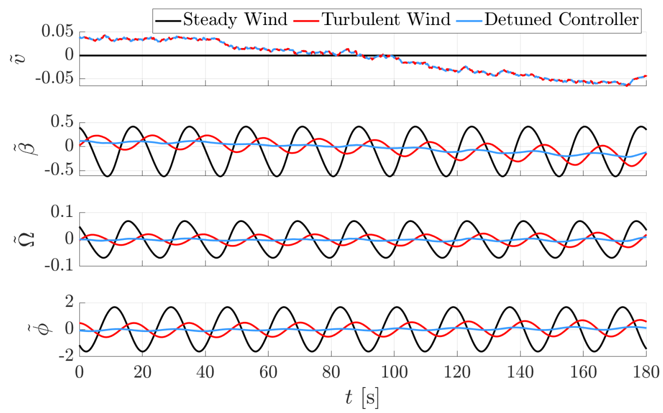

Fig. 8. Time-series plots of FOWT behavior simulated using a 2-DOF nonlinear model. The black curve was simulated under steady inflow wind at $\overline{v} = 14$ m/s with a high-gain blade-pitch PI controller, leading to a locally unstable equilibrium point (see Fig. 9). The red curve uses the same controller simulated under turbulent inflow at 6% turbulence intensity. The blue curve was simulated under the same turbulent inflow with a detuned blade-pitch controller. The y-axis scale on each plot is normalized.

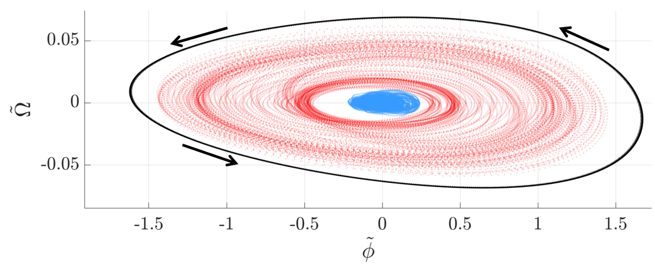

Fig. 9. The flattened $\phi - \Omega$ phase-plane of the simplified nonlinear FOWT model simulated in the cases from Fig. 8 for one hour of simulation time. The steady-inflow case results in a constant-amplitude periodic limit cycle (black). Under turbulent inflow (red), the amplitude of oscillations is reduced. With a stably detuned controller (blue), the state trajectory remains near the equilibrium despite turbulent inflow.

detriment to reference tracking bandwidth. Feedback of platform motion is a natural extension to the baseline controller that is easily modeled in the state-space representation (14). In this work, auxiliary control loops feeding back platform pitch rate $\dot{\phi}_{\text{ptfm}}$ (nacelle velocity $\dot{x}_{\text{RNA}}$ is equivalent if a rigid tower is assumed) to the turbine control inputs are called platform feedback (PF). The same control approach has been referred to as floating feedback [53], tower feedback [12], and nacelle feedback [46] in the literature. Platform feedback loops are used to drive the blade pitch and generator torque with gains k_{PF}^{β} and k_{PF}^{τ}, respectively:

$$\begin{bmatrix} \beta_{\text{PF}} \\ \tau_{\text{PF}} \end{bmatrix} = \boldsymbol{K}_{\text{PF}}\dot{\phi} = \begin{bmatrix} k_{\text{PF}}^{\beta} \\ k_{\text{PF}}^{\tau} \end{bmatrix} \dot{\phi}. \tag{16}$$

Multi-loop FOWT control methods are described in detail in [17]. To analyze multi-loop controllers, the auxiliary loops are first closed in an inner loop around the plant (14), with the primary controller (6) acting in an outer loop. After $\boldsymbol{K}_{\text{PF}}$ is padded with zeros to match the dimensions of $\boldsymbol{u}$ and $\boldsymbol{x}$, the inner-loop system matrix becomes

$$\begin{aligned} \boldsymbol{A}_{\text{inner}} &= \boldsymbol{A} + \boldsymbol{B}\boldsymbol{K}_{\text{PF}} \\ &= \left[\begin{array}{c|cc} A^{\Omega} & 0 & A_{\phi}^{\Omega} + k_{\text{PF}}^{\beta}B_{\beta}^{\Omega} + k_{\text{PF}}^{\tau}B_{\tau}^{\Omega} \\ \hline 0 & 0 & 1 \\ A_{\Omega}^{\phi} & A_{K}^{\phi} & A_{D}^{\phi} + k_{\text{PF}}^{\beta}B_{\beta}^{\phi} \end{array}\right]. \end{aligned} \tag{17}$$

The gains k_{PF}^{β} and k_{PF}^{τ} have tuning objectives based on a desired change to the natural parameters A_{D}^{ϕ} and A_{ϕ}^{Ω}.

1) Blade-Pitch Platform Feedback: From the structure of $\boldsymbol{A}_{\text{inner}}$ (17), blade pitch PF has influence on both the platform-generator coupling A_{ϕ}^{Ω} and the platform-DOF damping A_{D}^{ϕ}. To minimize platform motion and generator speed variation, we would like the magnitude of the former small (low coupling) and the latter large (high damping). Some tuning approaches attempt to compensate for this coupling [21, 36, 45, 46, 51, 54] while ostensibly reducing the platform damping as a result, although filtering of the feedback signal in the control loop complicates these analyses. Using an opposite-signed feedback gain increases platform pitch damping in A_{D}^{ϕ} [16, 17, 51]. In doing so, platform oscillations (and associated structural loading) are reduced, but the remaining platform motion has its torque influence on the generator-speed control loop slightly amplified.

Filtering the output signal may improve the viability of this feedback loop further by restricting action to certain frequencies [36]. Care should be taken to ensure that the filtered phase offset does not distort the design from the goal.

2) Generator-Torque Platform Feedback: Platform feedback to generator torque can be added to a generator-speed primary control loop to reduce the platform-generator coupling A_{ϕ}^{Ω} in $\boldsymbol{A}_{\text{inner}}$ (17). The generator torque PF loop utilizes an input and output distinct from the primary control loop, so this control loop has the name "parallel compensation" [14, 16, 17, 21, 51, 55]. Such a feedback loop is capable of relocating not only the poles of the inner-loop system (Fig. 6) but also the zeros, which are outside the influence of a shared-loop controller. With high enough gain k_{PF}^{τ}, the NMPZs responsible for instability can be moved completely into the left half-plane (LHP) to allow an increase in the primary controller bandwidth without becoming unstable.

The effect of parallel compensation on NMPZs can be seen as a modification of the coefficient μ_{aero} (15) [51]:

$$\mu_{\text{aero}}^{\text{comp}} = \frac{\partial F_{\text{aero}}}{\partial v} - \left(\frac{\partial T_{\text{aero}}}{\partial v} - k_{\text{PF}}^{\tau}\frac{N_{\text{gb}}}{H_t}\right)\frac{\partial F_{\text{aero}}/\partial\beta}{\partial T_{\text{aero}}/\partial\beta}. \tag{18}$$

The green curve in Fig. 7 shows $\mu_{\text{aero}}^{\text{comp}}$ tuned with parallel compensation gain $k_{\text{PF}}^{\tau} = 0.3 \cdot \frac{H_t}{N_{\text{gb}}}\frac{\partial T_{\text{aero}}}{\partial v} > 0$. The plot shows that the range of wind speeds where NMPZs are present is reduced compared to the baseline, and at wind speeds where $\mu_{\text{aero}}^{\text{comp}} < 0$, the NMPZs are moved into the LHP regardless of the value of D_{ϕ}.

Since the generator torque is already set to its rated value τ_{rated} in the baseline controller, the allowed feedback signal magnitude must be limited to avoid generator damage from sustained excess of rated power. A typical maximum torque input threshold is between 110% and 120% of τ_{rated} [14, 39], which in turn places a restriction on the maximum feedback gain k_{PF}^{τ} to avoid triggering

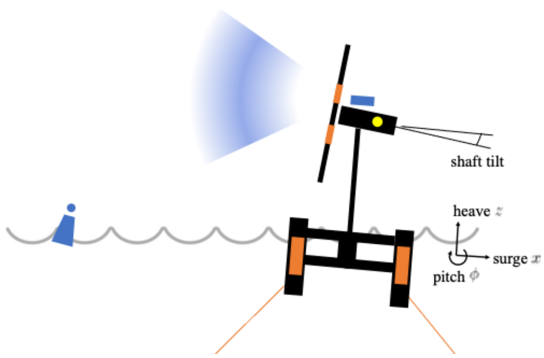

Fig. 10. Depiction of advanced controls concepts discussed. Orange elements are advanced actuators, including individual pitch motors, buoyancy cans, and mooring lines; blue elements are preview sensors, including lidar and buoys; and the yellow dot represents optimal control software. The xz-plane degrees of freedom of x-directional surge, z-directional heave, and pitching about the y-axis of the platform are also shown.

this nonlinear saturation unmodeled in (17). In addition, the PF control signal peaks and troughs are frequently aligned with generator speed oscillations, and combined they cause significant variations in generator power [17]. Despite improved performance in generator-speed regulation, the associated degradation of power quality caused by parallel compensation may not be acceptable for some designs.

Combined with blade-pitch PF that increases both platform damping and dynamic coupling, generator-torque PF can be used to mediate some of the increased coupling. Generator-torque PF without blade-pitch PF can also increase platform damping if combined with a power-regulating primary control loop [17, 56], although this is a lesser-studied feedback configuration. If the controller design is admitted greater complexity or additional hardware sensors or actuators, then a door opens to pursuing more advanced control approaches.

IV. Advanced Techniques for FOWT Control

Having described the main characteristics of the FOWT control problem and the "standard" control approaches, we turn to a discussion of "advanced" FOWT control methods. We discuss three main topics of interest (see Fig. 10): *advanced actuation*, referring to the deployment of new actuators on the FOWT or the exploitation of additional degrees of freedom in existing actuators; *preview sensing*, referring to the use of additional sensing equipment to take remote measurements of incoming disturbances and act accordingly; and *optimal control*, referring to the formulation of controllers that minimize certain multi-objective cost functions. Many studies have used two or all three of these elements. Advanced methods should not be treated as necessarily better than standard ones—the benefits of the advanced methods discussed here should be balanced against the cost of added complexity when selecting a controller.

A. Advanced Actuation

The added dynamics of FOWTs compared to their fixed-bottom counterparts call for the exploration of new methods of actuation. We describe here advances in blade actuation and the addition of controllable elements to the platform.

Individual-Blade Pitch Control (IPC): The earlier 1-DOF wind turbine model (4) assumes that the inflow wind v is uniform. In reality, the atmospheric boundary layer causes wind speed variations across the wind turbine rotor plane, leading to fluctuations in the output power, asymmetric loading on the rotor, and, in the case of FOWTs, increased platform motion. As each blade sweeps across the rotor plane, the aerodynamic torque and thrust it conveys to the RNA is dependent on its angular position around the central axis, the azimuth angle. In contrast to collective pitch control (CPC) which was assumed above, where all blades are pitched to the same degree β, IPC pitches each blade using distinct azimuth-dependent control commands. Benefits of IPC for FOWTs typically come from better power regulation, reduced platform motions, and decreased fatigue loading resulting in longer turbine lifetimes. For example, as rotors become larger, wind shear has an increasing effect on periodic loading on the blades and tower. This can be minimized by using IPC to target the once-per-revolution (1P) loads on the blades. Common IPC strategies achieve this by using the multi-blade coordinate (MBC) transformation [57] to convert blade loads from the rotating reference frame of their measurement to a fixed, non-rotating reference frame of the rotor plane. A differential pitch control demand is then calculated about the vertical and lateral axes of this fixed reference frame using multivariable control techniques or independently along each axis using multiple single-input, single-output (SISO) PI controllers, converted back to the rotating reference frame using inverse MBC and superimposed on the collective pitch demand which is driven by the rotor speed regulation objective [58].

In [59], a linear quadratic regulation (LQR) based IPC is presented for a FOWT. Periodic IPC is used to reduce power fluctuations as a primary objective and minimize platform motions and tower fatigue loading as secondary objectives. The periodic feedback gain changes in magnitude and sign as a function of the blade azimuth angle, creating asymmetric thrust loading on the rotor to generate a restoring platform pitching moment. A comparison between the LQR-based IPC, a baseline gain-scheduled CPC, and a full state-feedback-based CPC shows over 30% reduction in power fluctuations, over 40% reduction in platform pitching motion, and a nearly 40% decrease in tower side-to-side fatigue loading [59]. See Section IV-C for more on LQR.

Another approach to IPC uses nonlinear model predictive control (NMPC) to reduce blade loads caused by vertical and horizontal wind shear [60]. Intended for above-rated operation, the NMPC cost functional is designed to minimize deviations from rated generator speed and power (the primary objective of the baseline controller), platform surge and pitch rates, blade-pitch and generator-torque actuator usage, and the rotor yawing and pitching moments that contribute to the blade loads. Constraint equations are used to impose actuator position and rate limits to ensure feasible operation. Comparisons of NMPC against baseline control using full nonlinear aero-elastic simulations have shown NMPC to reduce out-of-plane and flapwise blade bending fatigue loads by 18% while reducing generator speed and power deviation by over 75% [60]. See also Section IV-C for more details on model predictive control.

Deformable Trailing Edge Flap (DTEF) Control: The unavoidable cost of IPC is the significantly higher blade pitch travel. This causes increased wear on pitch drive motors and pitch bearings of the blades. Recent research has explored the use of DTEFs to reduce fatigue loading on critical FOWT components [61–63]. The DTEF is an actively controlled airfoil element installed along a section of the blade span (usually near the tip) at the trailing edge. DTEF control dynamically alters the aerodynamic properties of the blade by changing the lift profile, similar to an aileron on an airplane wing. While DTEFs have been extensively studied for onshore wind turbines within the research community [64], their benefit to FOWT systems calls for more investigation.

The control strategy for DTEFs is often similar to that of IPC. Typical control objectives include reduction in periodic blade loading to minimize fatigue or reduction in power fluctuations and platform motion to improve power quality and reduce structural loading. This is achieved by individually pitching the DTEF of each blade using feedback from blade loads, rotor azimuth position, platform motion, or a combination of these. Initial studies show potential for DTEFs to achieve a significant reduction in loads and platform motions [61–63]. DTEFs offer efficient, high-bandwidth control with actuators that are smaller and consume less power as compared to blade pitch drives. However, installing DTEFs include major modifications to the blade and actuator mechanisms compared to a conventional FOWT.

Another alternative to full-blade IPC is segmented blades, where the entire outer segment of the blade can be pitched separately to the inner segment [65]. To our knowledge, this has not been investigated for FOWTs.

Platform Control: Undesired motions of the floating platform can be targeted directly by including additional mechanical components to the nacelle [66], platform [67], or mooring system [68]. Platform control involves using these actuators to augment the turbine controller and improve FOWT operation. Acting independently from the turbine controller allows the platform controller to operate while the turbine is parked (including in extreme wind and wave scenarios where its influence may be most beneficial [67]), and controlling the platform independently reduces the need for the turbine controller to regulate loads [8]. While standard wind turbine actuators (blade pitch, generator torque) that utilize rotor aerodynamic forces exhibit poor controllability of the platform roll mode [40, 53], most dedicated platform controllers need not rely on the rotor direction or the wind direction at all. The inclusion of multiple platform-control devices is not mutually exclusive, so complementary approaches may be combined to provide complementary control of relevant dynamics of the platform at multiple timescales (though doing so may be cost-prohibitive).

Platform actuators apply forces to the platform, typically at a lever-arm displacement, to influence platform rotation via applied torque. Platform controllers can be subdivided into *passive* (requiring no outside energy input, e.g., mass damper) and *active* (driven by some electro-mechanical actuator, e.g., active tensioner) methods. Passive methods are simpler, but their influence on platform dynamics is fixed by design parameters at manufacture and less flexible in capability. Active methods require control algorithm design, but they can adapt to a wider variety of environmental disturbance conditions that the system may encounter over its lifetime. Additionally, *semi-active* methods utilize passive components with dynamically adjustable parameters to track a changing optimal design configuration [66, 67, 69]. Actuator bandwidth is a critical consideration for active control methods. In general, a trade-off exists between control bandwidth and actuator power consumption, and certain actuator types have practical limitations on feasible bandwidth as well.

The family of structural control approaches is largely derived from techniques developed in civil engineering research to reduce vibrations in large structures [66, 70] and is here considered a subset of platform control. Structural vibrations at the natural frequency of one or more modes of platform motion can be dissipated by a resonating damped-mass system that may be actively controlled or consist of only passive components (that may be semi-actively adjustable). The simplest passive structural damper design is the tuned mass damper (TMD), which consists of a suspended mass with spatial perturbations restored by a spring (or spring-analog, e.g. pendulum) tuned to the desired resonant frequency and velocity damped by dissipative elements [66]. A properly designed TMD reduces the peak amplitude of the frequency response of a structure to disturbances, and has been applied successfully in tall structures for decades [70]. The design can be made more robust to changing conditions by adjusting TMD spring and damping parameters during operation in a semi-active manner, either continuously or in a quasi-discrete (on/off) manner. A fully active version of the TMD concept uses force drivers and a closed-loop controller to supply restoring and damping forces, possibly combined with some passive mechanical components in a hybrid approach [66]. Some related technologies utilize a sloshing liquid in a contained vessel, weight and buoyancy forces, and hydraulic pressure or viscosity as an analogous mass-spring-damper system to achieve a similar result as a TMD with a mechanically simpler device [66, 70].

In contrast to the small-amplitude, high-bandwidth use-case of a structural vibration absorber, actuators designed to control the steady-state settling point of the platform must apply forces at the same order of magnitude as the natural weight and buoyancy of the platform. Actuators that can feasibly influence the steady-state platform forces generally operate at a very low bandwidth compared to the wind turbine controller, with a response time on the order of ten minutes to an hour [21, 71]. One approach to low-bandwidth platform control for semisubmersible platforms is to actively add, remove, or redistribute water ballast in the floating substructure. Since a semisubmersible is stabilized by buoyant elements separated from the center of gravity, the platform tilting response can be controlled by changing the ballast in each element and the platform bouyancy distribution [71]. This approach can alleviate structural loads on the tower due to average and extreme platform tilting [21], increase below-rated power capture by compensating for rotor shaft tilt (see Figs. 5 and 10), or vertically deflecting the downstream wake (see also Section V).

B. Preview Sensing

While feedback control can be effective at reducing the impact of wind and wave disturbances, there is an inherent delay in the feedback system because the effect of the disturbance on, for instance, the rotor speed must be measured before control action can be taken to mitigate it. This delay is amplified by lags in the wind turbine actuators. There has been significant research interest in the past two decades into "feedforward" control approaches, which use preview measurements to actuate in anticipation of oncoming disturbances [72]. For instance, lidar scanners can sample the wind field upstream of the turbine to provide a measurement of upstream wind speed [73], which can improve rotor speed tracking compared to feedback control alone [74]. Feedforward controllers use a disturbance input model, which represents the impact of the disturbance on the system dynamics. The model is incorporated in the control design and is inverted either explicitly [59] or implicitly [75] to generate control actions that counteract the effects of disturbances as they arrive.

The use of lidar wind speed preview is well-established in the wind turbine control literature [72]. Several FOWT control papers utilize wind speed preview to improve rotor speed regulation performance and reduce platform motions [76, 77]. In nacelle-mounted lidar configurations (device depicted by the blue rectangle and scan location depicted as the blue shaded area in Fig. 10), corrections should be made to the lidar measurements to account for nacelle motion due to platform pitching [74].

On the other hand, wave preview has only recently found use in FOWT control. Observing and predicting oncoming waves is in some ways an easier problem than wind preview (if the long-upstream wave field can be directly observed using radar or lidar). While the sea state itself is composed of a stochastic frequency distribution, its propagation can be well approximated by linear dynamics with deterministic frequency-dependent energy and phase evolution [78]. While statistical (phase-averaged) prediction of the sea state over long timescales is an aspect of meteorology, deterministic (phase-resolved) sea wave prediction was first investigated for planning sensitive maritime activities that required foreknowledge of the envelope of wave disturbance amplitudes on shorter timescales [79]. Using the measured and propagated phase and frequency of incoming waves and a model of the FOWT system's frequency response to wave disturbances, turbine actuators can be controlled in a feedforward manner to mitigate the impact of the disturbance on system outputs [80]. The forward-propagation of the wave disturbance is highly deterministic over a longer range than inflow wind turbulence [78], allowing for a wider variety

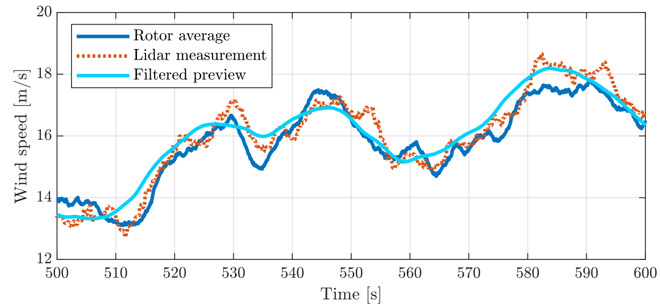

Fig. 11. Simulated lidar measurements of horizontal wind speed. The dark blue line is the true, rotor average wind speed that impacts the turbine, based on a FAST simulation [81]; the orange dotted line is the simulated lidar-measured horizontal wind speed; and the light blue line is a smoothed version of the lidar measurement using a moving average smoother.

of useful wave measurement approaches (e.g., sensor buoys upstream from a floating wind farm) and the potential of disturbance measurements to remain useful even after they have encountered an upstream FOWT.

The majority of works that consider disturbance preview and feedforward controls for wind turbines assume perfect knowledge of future disturbances. In practice, disturbance measurements are likely to be inaccurate due to both sampling imperfections and evolution of the wind/waves as they move from the measurement location to the turbine location (see Fig. 11). Studies considering these types of imperfections include modeling of imperfect wind speed measurements from lidar [74] and comparisons of forecasting techniques to make predictions of future wave behavior based on (perfect) measurements at the turbine location [75].

C. Optimal Control Approaches

As described in Section III, there are inherent trade-offs between rotor speed tracking performance, structural loading, and actuator usage. Tuning control gains to heuristically balance these objectives may be time-consuming and heavily dependent on expert knowledge, especially when there are multiple interacting feedback loops. An alternative approach is to use optimal control, where a global cost function is constructed from a weighted combination of individual terms, each relating to a different control objective. Solving the resulting optimization problem yields the optimal controller. The tuning challenge remains—the control designer must choose various weights in the cost function—but the optimal control framework does allow for a systematic control design procedure and, arguably, an easier interpretation of the parameters being tuned.

Optimal controllers are often used in conjunction with advanced actuation approaches [82] or preview-enabled control [83], but can also be used as a direct replacement for nonoptimal control approaches. We split the discussion of optimal controllers into those that can be found in closed-form via an offline procedure, and model predictive control, which in general does not have a closed-form solution and requires solving an optimization problem online.

Closed-form Controllers: Historically, perhaps the most popular optimal control approach is LQR. The continuous-time, infinite-horizon LQR problem is to minimize the quadratic cost function

$$\mathcal{J} = \int_0^\infty \left(\boldsymbol{x}^\top \boldsymbol{Q} \boldsymbol{x} + \boldsymbol{u}^\top \boldsymbol{R} \boldsymbol{u} \right) \, dt \tag{19}$$

subject to $\dot{\boldsymbol{x}} = \boldsymbol{A}\boldsymbol{x} + \boldsymbol{B}\boldsymbol{u}$. Matrices $\boldsymbol{Q}$ and $\boldsymbol{R}$ represent weights assigned to individual cost function terms. The optimal solution is a state feedback law $\boldsymbol{u}^\star = -\boldsymbol{K}\boldsymbol{x}$, where the time-invariant gain matrix $\boldsymbol{K}$ can be found offline.

LQR has been applied for FOWT control, both for full MIMO controller replacement [77] or for replacing portions of the controller [84, 85]. LQR has been used to balance tracking performance with structural loading [85]. The effect of varying the cost function weights in the LQR formulation has also been studied to evaluate the trade-off between tracking performance and actuator usage [84]. LQR has also been extended to handle preview wave disturbances [75]. A periodic formulation of the LQR problem allows for reducing asymmetrical loads on the rotor (see Section IV-A for details).

The canonical LQR formulation relies on a linear, time-invariant model and assumes that the full state is available for feedback. While many authors assume that sensors are available to directly measure the entire state, in general, state feedback controllers must be paired with state estimators. The combination of appropriate state estimators with LQR controllers (e.g., linear-quadratic-Gaussian control) for FOWTs is an area of possible future research.

On the other hand, the $\mathcal{H}_\infty$ formulation has been used to design robust, dynamic output-feedback controllers directly, at the cost of a somewhat more involved design procedure [86]. The $\mathcal{H}_\infty$ control framework shapes the frequency response of the closed-loop system as desired to address the various trade-offs as well as uncertainties in the plant model. The $\mathcal{H}_\infty$ formulation can also be expanded to handle linear parameter-varying model representations [84, 87], which is useful to help capture the nonlinearities present in FOWTs.

Model Predictive Control (MPC): The FOWT literature shows several MPC studies. Consider an optimal control problem with the general form

$$\begin{aligned} &\text{minimize} \int_t^{t+T} c(\boldsymbol{x}, \boldsymbol{u}) \, dt && \text{(20a)} \\ &\text{subject to} \quad \dot{\boldsymbol{x}} = f(\boldsymbol{x}, \boldsymbol{u}), \quad \boldsymbol{x} \in \mathcal{X}, \quad \boldsymbol{u} \in \mathcal{U} && \text{(20b)} \end{aligned}$$

where T is a (usually finite) prediction horizon , c is a general cost function, f is a general dynamical model, and $\mathcal{X}$ and $\mathcal{U}$ are the constraint sets that the state and control input are allowed to evolve in, respectively. The LQR problem (19) is an optimal control problem where c is a quadratic function, f represents the linear dynamics, the constraint sets are simply the entire state and input spaces, and the horizon T is infinite.

While the LQR problem has a closed-form solution, most optimal control problems do not. In MPC, the optimization problem (20) is discretized in time and solved online for each new measurement (or estimate) of the state $\boldsymbol{x}(t)$. This produces a sequence of optimal control actions $\{\boldsymbol{u}\}^\star_{t:t+T}$, the first of which is applied to the system; once a new state measurement is available, the problem is re-solved for the next control action. Note that care must be taken to ensure that a feasible solution to the problem can be found if state constraints in (20b) are being used.

MPC has been used for a range of FOWT studies. A distinction between these is the choice of model representation f, from nonlinear representations of the wind turbine [83] to linear time-invariant [88] and linear parameter-varying [76] representations. An interesting middle ground uses switching and hybrid models, where a family of linear representations is used in the MPC problem [89]. MPC has been primarily used for above-rated operation, where mitigating structural loading is important; however, several studies consider the design of MPCs that can handle below- and above-rated operation, as well as the transition between them [89, 90]. Nonstandard implementations include [88], which considers using MPC for IPC (see Section IV-A) after a blade pitch actuator failure.

MPC has received attention due to its ability to naturally handle preview disturbance information (see Section IV-B). If the disturbances $\boldsymbol{w}(t)$ are known (or forecast) over the prediction horizon, the model in (20b) can be replaced with a model including the exogenous input, i.e., $\dot{\boldsymbol{x}} = f(\boldsymbol{x}, \boldsymbol{u}, \boldsymbol{w})$. The controller design is, in principle, unchanged, except that now the optimal control sequence $\{\boldsymbol{u}\}^\star_{t:t+T}$ accounts for the oncoming disturbances and their effects on the predicted states. Note that the cost function (20a) may need to be retuned to make the best use of the extra information. Examples of MPC formulations that make use of preview disturbance information can be found in [83, 91, 92].

A drawback of MPC, compared to other optimal controllers such as LQR and $\mathcal{H}_\infty$ control, is that an optimization problem is solved online at every time step (an exception is explicit MPC [85], but this tends to be limited to small state spaces). Online optimization usually requires an iterative solution approach and thus significant computational resources. An ongoing challenge is the ability to solve the MPC problem quickly enough for real-time implementation at the controller update rate of modern wind turbines, typically 10–100 Hz [39]. For only blade pitch control, which tends to have slower dynamics than the generator power electronics, it may be possible to solve the MPC problem at a lower sampling rate [83, 92]. Additionally, theoretical guarantees of stability and robustness are more difficult to obtain for MPC than LQR and $\mathcal{H}_\infty$ controllers.

Factors influencing MPC performance include the model used for controller development, the choice of cost function, and constraints used. To understand the importance of various decisions made in the MPC design process, competing MPCs must be compared side-by-side, and there appear to be only a few such studies. In [93], comparisons are made across approaches for obtaining the linearized model as well as between preview-enabled and non-preview-enabled MPC. MPC performance under different choices of cost function weights is considered in [19]. It is natural for separate studies formulating MPC to appear first, but a critical next step is the development of further comparative studies.

V. Floating Offshore Wind Farms

A. Problem Description

There are currently four floating offshore wind farms (FOWFs), each with only 3 to 11 wind turbines [6, 94]. As the technology matures, ultimately, like land-based and fixed-bottom wind farms, FOWFs with many (>30) FOWTs will be installed. Similar to their land-based and fixed-bottom counterparts, a goal in the design and control of FOWFs is to achieve a farm-level objective such as tracking a total time-varying power reference or maximizing farm-wide power production, by coordinating the design parameters and operational control set points of the individual wind turbines. Challenges arise due to wake effects. When wind turbines operate in a wind farm, wakes are generated behind the upstream wind turbines. This results in a wind field with greater turbulence and reduced velocity for the downstream wind turbines [95]. Compared to land-based sites, the wind field in offshore sites exhibits lower turbulence intensities, which on the one hand results in decreased structural loading on the wind turbines, but on the other hand results in a longer wake recovery period due to decreased mixing [96].

The baseline wind farm control approach is known as greedy control, where each wind turbine is oriented directly into the wind and is controlled to maximize its individual power output. This strategy leads to downstream turbines producing less power due to wake effects. The goal of wind farm control is thus to adjust the set points, orientations, and locations of individual wind turbines to achieve the farm-level objective while accounting for wake effects. This is a complex, non-convex optimization problem with many local optima, and land-based and fixed-bottom wind farm controls has already been an active research area [22–28].

In this section, we provide an overview of particular issues and methods that can be used to control FOWFs, though in some cases much of the existing literature has been focused on land-based or fixed-bottom wind farms.

B. Modeling

Model-based wind farm controller design and validation requires accurate and computationally efficient wake models. Land-based and fixed-bottom wind farm wake modeling research is ongoing [97], and research into the effects of floating platforms on wakes is in its infancy [98]. Initial wind tunnel experiments were conducted to study the influence of streamwise turbine platform motion on wake development [99]. A low-fidelity dynamic parametric wind farm model is presented in [100] for simulating platform motion and wake transport of FOWTs under time-varying wind conditions. The model is validated against experimental wind-tunnel data and high-fidelity simulations. However, there is still a lack of high-fidelity (large-eddy simulation, or LES)-based simulators that capture floating platform dynamics, which is important for validating low-fidelity models. Existing and upcoming tools are described in Section VI-C. In general, more studies including field validations are needed to better understand the wake characteristics of FOWTs.

C. Control Methods

To mitigate power loss and uneven fatigue distribution due to wake effects, three types of FOWF control methods have been studied: induction control (IC) [30, 101, 102], wake deflection (or steering) [29], and platform relocation [103–105]. These methods are reviewed in the following sections and are depicted conceptually in Fig. 12.

1) Induction Control (IC): IC (power derating) varies wind turbine axial induction factor (AIF) set points from their power-maximizing values. The AIF represents the fractional decrease in wind velocity between free stream conditions and those at the rotor plane. The generator-torque and blade-pitch controllers are adjusted to achieve a particular AIF set point.

IC can be further categorized into static induction control (SIC) and dynamic induction control (DIC). In SIC, the upstream turbine AIFs are fixed at lower values by design. Reducing the AIF of a turbine reduces its individual power but increases the wind speed in its wake and thus the power available to downstream turbines, and SIC has been shown to improve both power reference tracking [106] and power maximization [107]. In DIC, the wind turbine AIFs are varied in order to increase mixing in the wakes so that wind speeds recover more quickly to their freestream levels. DIC methods have been explored with both CPC and IPC [102, 108]. DIC via CPC uses a periodic collective blade pitch command to create a periodic "pulse" in the wake behind the turbine. DIC via IPC, also known as the helix method due to the helical shape of the resulting wake, uses IPC to increase mixing, which leads to greater wake turbulence and faster wake recovery. These IC approaches are depicted in Fig. 12.

2) Wake Deflection: Wake steering achieves a power maximization objective by either changing the yaw angle (i.e., lateral wake deflection or yaw misalignment) or the pitching attitude of the platform (i.e., vertical wake steering) of upstream wind turbines to redirect the generated wake away from downstream turbines. Lateral wake deflection via intentional yaw misalignment has been studied in the control of land-based and fixed-bottom wind farms [22–28]. However, there seems to be little research available on FOWF-specific lateral wake steering control, likely due to lack of knowledge on how wakes dissipate behind FOWTs. As more FOWT wake models are developed and validated, this area of research is expected to grow quickly.

Vertical wake deflection involves tilting the rotor in the fore-aft direction, such as by transferring water ballast between the columns of the floating platform. The feasibility of vertical wake deflection for FOWTs using differential ballast control is investigated in [29]. The key finding is that steering the wake towards the sea surface ('wake-down') results in greater farm-level power gains as compared with steering the wake towards the sky. The choice of configuration parameters for this method include geometric characteristics of the platform-turbine assembly, turbine orientation with respect to the platform, and the location of the turbine tower base with respect to the platform center of flotation [29]. Further research is needed to establish the comparative costs,

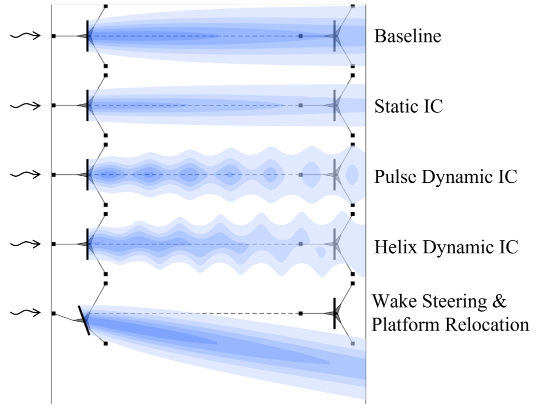

Fig. 12. Top-down view of a floating offshore wind farm (FOWF), with wind inflow from left to right, depicting the wake deficit caused by an upstream turbine using FOWF control methods. The arrows show the inflow wind direction, and darker colors show a larger wind-speed deficit in each upstream turbine wake. Due to wake mixing, the deficit is largest immediately behind the rotor and returns towards the freestream speed as the wake expands and flows downstream. From top to bottom: Baseline greedy control at power-maximizing induction factor; static IC with reduced initial deficit; pulse and helix dynamic IC, both with faster wake recovery; lateral wake steering with platform relocation that causes the wake to avoid the downstream turbine altogether. Vertical wake deflection (not shown) would be directed perpendicular to the image plane.

benefits, and optimal integration of vertical and lateral wake deflection for the purposes of wake manipulation in FOWTs.

3) Platform Relocation: As long as the mooring lines of a FOWT are not taut, the FOWT may be relocated (within a constrained region) during operation in response to changing wind conditions to mitigate wake effects. This can be achieved directly with additional actuators or indirectly by utilizing the aerodynamic forces acting on the wind turbine and the standard (generator torque, blade pitch, and yaw) actuators. FOWT configuration parameters that affect platform relocation capabilities include the lengths of the mooring lines and how far the mooring system anchors are from the nominal turbine locations [109] (i.e., the originally designed platform locations). While platform relocation [104, 105] has been explored, further research is needed to better understand the trade-offs between increased performance (higher power capture and reduced structural loading) and costs (of longer mooring lines and potentially higher structural loads in some components during the platform maneuvering process). Platform relocation and wake deflection are both depicted together in Fig. 12.

Given the limited radius of platform relocation, there is strong potential for the application of control co-design methods. Control co-design is an approach in which system design and control design are performed in an iterative and parallel fashion, as opposed to the more traditional sequential workflow [41]. Specifically, this involves optimizing mooring line lengths, nominal platform locations, platform orientations and configurations for real-time relocation in parallel with real-time controller tuning. Froese et al. presented their findings on the design-phase optimization [103], and further gains in farm-level power and reductions in cost could be achieved by integrating this research with real-time relocation control optimization research [104, 105].

VI. Tools & Experiments

In recent years, a number of advanced modeling tools have emerged to enable the research and development of floating offshore wind energy systems. These tools range in fidelity levels and, concurrently, the methods by which the control system is integrated into the tool itself. Though there have been countless toolsets developed by research institutions and corporate entities across the globe, in this section we focus on toolsets that satisfy at least one of the following criteria:

a) An actively maintained open-source toolset that is currently available for public access and use.
b) A commonly used commercial software that is pervasive in the field and used extensively for design and certification of wind turbines.

A. Floating Offshore Wind Turbine Modeling

The National Renewable Energy Laboratory (NREL) actively develops and maintains OpenFAST [110] as its primary tool for modeling and simulation of wind turbines. OpenFAST, an extension of the older FAST [81] code, has become ubiquitous for simulation of both land-based, fixed-bottom offshore, and floating offshore wind turbine models in the academic and commercial sectors. OpenFAST is a "multi-physics, multi-fidelity" time-domain-based tool for simulation of the dynamic response of floating wind turbines.

A similar simulation tool, HAWC2 [111], has been developed at DTU. HAWC2 is available free of charge for research purposes and follows a subscription-based license model for enterprise users. A recent study [112] provides a comparison of the response characteristics of a fixed-bottom offshore wind turbine using HAWC2 and OpenFAST.

To our knowledge, many commercial wind turbine developers actively use and maintain their own in-house modeling tools (in some cases, customized versions of open-source tools such as HAWC2 or OpenFAST). Some commercial enterprises do not have the resources to maintain their own in-house simulation tools. In this case, the leading commercial software for design and development of wind turbines is DNV-GL's Bladed [113]. Not only is Bladed used for design of wind turbines and their various components, but it is also used by the international certification bodies for the standardized load assessment and compliance certifications necessary to commission a wind turbine.

Though these three mentioned toolsets each contain hydrodynamic modeling modules for floating model simulation and analysis, the complexity of the marine environment often necessitates higher-fidelity tools for adequate analysis of the system. Orcina's OrcaFlex [114] is a package developed for dynamic analysis of marine systems. In recent years, the coupling between OrcaFlex and more wind-turbine-specific aero-elastic codes has improved and enabled a more comprehensive analysis of floating wind energy systems.

There has also been a push to develop lower-order modeling simulation tools to enable more rapid design and analysis of floating offshore wind turbines. NREL has recently distributed Response Amplitudes of Floating Turbines

(RAFT) [115], a quasi-static frequency-domain-based tool that can be used for rapid modeling of floating wind turbines. RAFT can be used to provide efficient computations of platform hydrodynamics and mooring system responses, rotor aerodynamics, and allows considering linearized feedback control systems. Other institutions have developed slightly higher-fidelity, linear-model-based tools such as the SLOW toolset [116] originally developed at the University of Stuttgart, though these are not publicly available.

B. Reference Controllers

The presence of a publicly available reference controller with specific features for floating offshore wind turbine applications was lacking until recently. The NREL 5 MW controller had previously been de-rated [44] to avoid the negative-damping issue in floating systems, but no additional controller modifications or development was done. Similarly, variations of the Basic DTU Wind Energy Controller [117] have been applied to floating systems, again without additional modifications.

The Reference Open-Source Controller (ROSCO) [36] has introduced a controller that enables modern control functionalities representative of industry practices. From a floating-systems perspective, ROSCO contains a compensation-based blade-pitch platform feedback loop to help stabilize floating systems. Additionally, the pitch-saturation (i.e., thrust-clipping) routine in ROSCO has also been shown to have a positive effect on the fore-aft damping of a floating wind turbine, helping to maintain system stability, though potentially at the cost of power output near rated. Finally, the ROSCO toolbox tuning processes also include stability-constrained controller tuning methods to guarantee stability of the linearized floating offshore wind turbine system [118].

The use of reference baseline controllers to compare FOWT control innovations is not standardized in the literature. Many published results compare against a fixed-bottom reference controller that may be destabilizing, and therefore significant performance improvements can be misleading. While readers should be aware of this caveat, the most appropriate baseline for a given work is context-dependent rather than imposing a common reference. A multitude of techniques now exist for stabilizing a baseline controller within a desired level of complexity, and FOWT control research is approaching a level of maturity where comparing against an unstable baseline is seldom appropriate.

C. Wind Farm Applications

NREL has also developed FLOw Redirection and Induction in Steady State (FLORIS) [119], an aerodynamic analysis tool for farm-level control system design. This tool facilitates active flow control and wake steering studies. Because the tool is rooted in steady-state analysis, the FOWT dynamics are not captured. NREL is in the process of incorporating FOWT-specific steady-state effects, such as mean platform tilt, into FLORIS. Farm-level dynamic simulation tools are useful for analysis and controller development for floating wind farms [98, 120]. An example is FAST.Farm [121], which couples the nonlinear single-turbine dynamic simulations of OpenFAST with farm-level wake interactions.

D. Experimental Campaigns

There have also been a number of experimental campaigns to test and validate control strategies for floating offshore wind turbines. Though this is certainly not an exhaustive list of publications regarding full- or scaled-model floating wind turbine testing, this section highlights a selection of experiments that either focus on the control system, or specifically address the role of the controller in the experimental results.

Experiments led by researchers at DTU have utilized a 1:60 scaled model of the DTU 10 MW wind turbine on a tension-leg platform (TLP) [122] and a Triple Spar floater [123]. In both studies, the tunings of the Basic DTU Wind Energy controller [117] for fixed-bottom and floating configurations are compared.

In two publications by Kakuya et al., the impacts of the controller on the tower and platform fore-aft vibrations are specifically investigated. A blade pitch-based vibration control method is assessed on a full-scale 2 MW floating wind turbine on a spar-type floating platform in [124]. The damping influence of adjusting the minimum generator torque based on nacelle speed is explored in [125] and is validated on the same full-scale 2 MW wind turbine model.

Advanced control methods are used in an experimental campaign by Hara et al. in [86], where a model-based $\mathcal{H}_\infty$ controller is used. The controller is applied to a 1:100 Froude-scaled (a common method of scaling offshore structures [126]) model of the NREL 5 MW wind turbine, and the ability of the controller to regulate platform pitch and rotor speed is assessed.

The Floating Offshore-wind and Controls Advanced Laboratory (FOCAL) project—funded by the US Department of Energy's ATLANTIS program [127]—has recently published results from their most recent experimental campaign [128]. In this study, the ROSCO controller was integrated with a 1:70 Froude-scaled model of the International Energy Agency (IEA) 15 MW reference wind turbine and simple controller performance was assessed. This study was the first step of a four-part campaign to complete scaled model testing of the IEA 15 MW turbine on a floating platform.

VII. Other FOWT Configurations

In addition to the prevalent HAWT designs, other FOWT configurations being investigated include vertical-axis wind turbines (VAWTs) and multiturbine platforms.

A. Floating Vertical Axis Wind Turbines

Although HAWTs now dominate the wind turbine industry, the earliest records of wind turbines are from the 9th century and describe simple Persian vertical-axis windmills based on aerodynamic drag [129]. VAWT designs based on aerodynamic lift have been explored since the 1920s [130]. A recent historical review of VAWTs indicates that the reasons some land-based VAWT projects have failed are due to problems with fatigue and durability [130]. HAWTs have experienced widespread commercial success in large part due their reliability. However, there are characteristics of VAWTs that may be beneficial for floating offshore wind energy systems [131–133]. VAWTs have a lower center of gravity and hence are more inherently stable. VAWTs can run their generators near the waterline, which means that they can be more easily maintained without the need for large cranes. VAWTs are also omnidirectional and hence do not need yaw drives. Further, VAWTs have smaller wake effects and can thus be deployed closer together than HAWTs. As a result, there is ongoing interest in VAWTs [132, 133], and studies are underway to determine if the fatigue and reliability issues that have previously hampered land-based VAWTs can be sufficiently addressed to enable the benefits of VAWTs for floating offshore wind applications to be realized.

B. Multi-turbine Platforms

Since the floating platform (and substructure) are a large fraction of the cost for floating wind turbines [134], multi-turbine platforms are being explored where multiple turbines are mounted on a single floating platform. While most multi-turbine platforms that have been investigated have a few turbines [135, 136], concepts with many ($>$100) turbines on a single platform have also been proposed [137]. Varying configurations are still being investigated, and it is unclear which concepts may emerge as being reliable and able to provide electrical energy at competitive costs.

VIII. Outlook

Fundamental research into FOWT control has helped resolve many initial challenges of floating wind energy technology through a diversity of control approaches. The forces enabling this decade's realization of the technology are a combination of government and business economics, public sentiment on renewable energy, and research ingenuity in both the plant design and controller.

While only 123 MW of floating offshore wind power was operational around the world as of December 31, 2021, projections indicate that cumulative floating offshore wind capacity could exceed 8 GW by 2027, representing a 65-fold increase in the next 5 years [6]. Five independent forecasts on floating offshore wind deployment from 2025 to 2050 show more than 10 GW by 2030 and up to 264 GW by 2050 [6]. This rapid increase in the scale of FOWT deployment will require research innovation to improve efficiency and longevity of FOWT systems. Vast growth also offers tools to aid the research community in solving the problems that arise along the way, in the form of full-scale experimental data on a diverse set of technologies. Stepping outside the traditional control design process by coupling the plant and controller design (also called co-design [41]) may continue to present opportunities for future progress beyond the simple adaptation of traditional wind turbine control.

These are promising forecasts that clearly suggest that the future of the floating wind turbine industry is bright. We hope that this tutorial helps provide the community with foundational knowledge of the many facets of FOWT control systems research and enables the next generation of floating offshore wind turbine technologies.

Appendix

The matrix elements of the linearized wind turbine model (14) are

$$A_{\phi}^{\Omega} = -H_t \frac{N_{\text{gb}}}{J_{\text{rot}}} \frac{\partial T_{\text{aero}}}{\partial v}, \quad A^{\Omega} = \frac{N_{\text{gb}}}{J_{\text{rot}}} \frac{\partial T_{\text{aero}}}{\partial \Omega}, \quad A_{\Omega}^{\phi} = \frac{H_t}{J_{\phi}} \frac{\partial F_{\text{aero}}}{\partial \Omega},$$
$$A_K^{\phi} = \frac{-K_{\phi}}{J_{\phi}}, \qquad A_D^{\phi} = \frac{-1}{J_{\phi}} \left(D_{\phi} + H_t^2 \frac{\partial F_{\text{aero}}}{\partial v} \right),$$
$$B_{\beta}^{\Omega} = \frac{N_{\text{gb}}}{J_{\text{rot}}} \frac{\partial T_{\text{aero}}}{\partial \beta}, \qquad B_{\tau}^{\Omega} = -\frac{N_{\text{gb}}^2}{J_{\text{rot}}}, \qquad B_{\beta}^{\phi} = \frac{H_t}{J_{\phi}} \frac{\partial F_{\text{aero}}}{\partial \beta}.$$

References

[1] www.whitehouse.gov/briefing-room/statements-releases/2021/04/22/fact-sheet-president-biden-sets-2030-greenhouse-gas-pollution-reduction-target-aimed-at-creating-good-paying-union-jobs-and-securing-u-s-leadership-on-clean-energy-technologies/, 2021, accessed Aug. 2022.
[2] R. Wiser, M. Bolinger, B. Hoen, D. Millstein, J. Rand, G. Barbose, N. Darghouth, W. Gorman, S. Jeong, and B. Paulos, "Land-based wind market report: 2022 edition," US Dept. of Energy Office of Energy Efficiency & Renewable Energy, Tech. Rep. DOE/GO-102022-5763, 2022.
[3] D. Feldman, K. Dummit, J. Zuboy, J. Heeter, K. Xu, and R. Margolis, "Spring 2022 solar industry update," US Dept. of Energy Office of Energy Efficiency & Renewable Energy, Tech. Rep. NREL/PR-7A40-82854, 2022.
[4] R. Uria-Martinez, M. Johnson, R. Shan, N. Samu, G. Oladosu, J. Werble, and H. Battey, "U.S. hydropower market report," US Dept. of Energy Office of Energy Efficiency & Renewable Energy, Tech. Rep. DOE/EE-2088, 2021.
[5] "Interior joins government-wide effort to advance offshore wind," www.doi.gov/news/interior-joins-government-wide-effort-advance-offshore-wind, 2021, accessed Aug. 2022.
[6] W. Musial, P. Spitsen, P. Duffy, P. Beiter, M. Marquis, R. Hammond, and M. Shields, "Offshore wind market report: 2022 edition," US Dept. of Energy Office of Energy Efficiency & Renewable Energy, Tech. Rep. DOE/GO-102022-5765, 2022.
[7] "Windeurope," https://windeurope.org, 2022, accessed Aug. 2022.
[8] K. A. Shah, F. Meng, Y. Li, R. Nagamune, Y. Zhou, Z. Ren, and Z. Jiang, "A synthesis of feasible control methods for floating offshore wind turbine system dynamics," *Renew. & Sustainable Energy Rev.*, 2021.
[9] J. Jonkman and D. Matha, "Quantitative comparison of the responses of three floating platforms," in *Proc. European Offshore Wind Conf. and Exhibition*, 2009.
[10] R. Damiani and M. Franchi, "An innovative second-order design method for the structural optimization of the Spider-FLOAT offshore wind platform," *Ocean Eng.*, 2021.
[11] T. J. Larsen and T. D. Hanson, "A method to avoid negative damped low frequent tower vibrations for a floating, pitch controlled wind turbine," *J. Phys.: Conf. Series*, 2007.
[12] J. Jonkman, "Influence of control on the pitch damping of a floating wind turbine," in *Proc. ASME Wind Energy Symp.*, 2008.
[13] G. van der Veen, I. Couchman, and R. Bowyer, "Control of floating wind turbines," in *Proc. Amer. Ctrl. Conf.*, 2012.
[14] B. Fischer, "Reducing rotor speed variations of floating wind turbines by compensation of non-minimum phase zeros," *IET Renewable Power Generation*, 2013.

[15] P. A. Fleming, A. Peiffer, and D. Schlipf, "Wind turbine controller to mitigate structural loads on a floating wind turbine platform," *J. Offshore Mech. and Arctic Eng.*, 2016.

[16] W. Yu, F. Lemmer, D. Schlipf, P. W. Cheng, B. Visser, H. Links, N. Gupta, S. Dankemann, B. Counago, and J. Serna, "Evaluation of control methods for floating offshore wind turbines," *J. Phys.: Conf. Series*, 2018.

[17] D. Stockhouse and L. Pao, "Trade-offs in the design of multi-loop controllers for floating wind turbines," *Proc. Amer. Ctrl. Conf.*, 2023.

[18] Z. Wu and Y. Li, "Platform stabilization and load reduction of floating offshore wind turbines with tension-leg platform using dynamic vibration absorbers," *Wind Energy*, 2020.

[19] ——, "Hybrid model predictive control of floating offshore wind turbines with artificial muscle actuated mooring lines," *J. Dyn. Sys., Meas., and Ctrl.*, 2022.

[20] E. Grant, K. Johnson, R. Damiani, D. Stockhouse, J. Dinius, M. Phadnis, and L. Pao, "Combined low-bandwidth platform actuation and floating feedback control for an offshore wind turbine with an ultraflexible substructure," in *Proc. Amer. Ctrl. Conf.*, 2022.

[21] D. Stockhouse, M. Phadnis, E. Grant, K. Johnson, R. Damiani, and L. Pao, "Control of a floating wind turbine on a novel actuated platform," in *Proc. Amer. Ctrl. Conf.*, 2022.

[22] P. Fleming, P. M. O. Gebraad, S. Lee, J.-W. van Wingerden, K. Johnson, M. Churchfield, J. Michalakes, P. Spalart, and P. Moriarty, "Simulation comparison of wake mitigation control strategies for a two-turbine case," *Wind Energy*, 2015.

[23] P. M. O. Gebraad, F. W. Teeuwisse, J.-W. van Wingerden, P. A. Fleming, S. D. Ruben, J. R. Marden, and L. Y. Pao, "Wind plant power optimization through yaw control using a parametric model for wake effects – a CFD simulation study," *Wind Energy*, 2016.

[24] P. Fleming, J. Annoni, J. J. Shah, L. Wang, S. Ananthan, Z. Zhang, K. Hutchings, P. Wang, W. Chen, and L. Chen, "Field test of wake steering at an offshore wind farm," *Wind Energy Sci.*, 2017.

[25] R. Damiani, S. Dana, J. Annoni, P. Fleming, J. Roadman, J. van Dam, and K. Dykes, "Assessment of wind turbine component loads under yaw-offset conditions," *Wind Energy Sci.*, 2018.

[26] M. Howland, S. Lele, and J. Dabiri, "Wind farm power optimization through wake steering," *Proc. Natl. Acad. Sci.*, 2019.

[27] E. Simley, P. Fleming, and J. King, "Design and analysis of a wake steering controller with wind direction variability," *Wind Energy Sci.*, 2020.

[28] M. F. Howland, J. B. Quesada, J. J. P. Martinez, F. P. Larranaga, N. Yadav, J. S. Chawla, V. Sivaram, and J. O. Dabiri, "Collective wind farm operation based on a predictive model increases utility-scale energy production," *Nature Energy*, 2022.

[29] E. M. Nanos, C. L. Bottasso, S. Tamaro, D. I. Manolas, and V. A. Riziotis, "Vertical wake deflection for floating wind turbines by differential ballast control," *Wind Energy Sci.*, 2022.

[30] D. van den Berg, D. de Tavernier, and J.-W. van Wingerden, "Using the helix mixing approach on floating offshore wind turbines," *J. Phys.: Conf. Series*, 2022.

[31] R. J. Barthelmie, K. Hansen, S. T. Frandsen, O. Rathmann, J. G. Schepers, W. Schlez, J. Phillips, K. Rados, A. Zervos, E. S. Politis, and P. K. Chaviaropoulos, "Modelling and measuring flow and wind turbine wakes in large wind farms offshore," *Wind Energy*, 2009.

[32] L. Y. Pao and K. E. Johnson, "Control of wind turbines," *IEEE Ctrl. Sys. Mag.*, 2011.

[33] T. Burton, D. Sharpe, N. Jenkins, and E. Bossanyi, *Wind Energy Handbook*. John Wiley & Sons, 2001.

[34] K. E. Johnson, L. Y. Pao, M. J. Balas, and L. J. Fingersh, "Control of variable-speed wind turbines: standard and adaptive techniques for maximizing energy capture," *IEEE Ctrl. Sys. Mag.*, 2006.

[35] D. Schlipf, "Set-point-fading for wind turbine control," 2019, Technical Presentation.

[36] N. Abbas, D. Zalkind, L. Y. Pao, and A. Wright, "A reference open-source controller for fixed and floating offshore wind turbines," *Wind Energy Sci.*, 2022.

[37] M. A. Lackner, "Controlling platform motions and reducing blade loads for floating wind turbines," *Wind Eng.*, 2009.

[38] D. Zalkind, E. Dall'Anese, and L. Y. Pao, "Automatic controller tuning using a zeroth-order optimization algorithm," *Wind Energy Sci.*, 2020.

[39] J. Jonkman, S. Butterfield, W. Musial, and G. Scott, "Definition of a 5-MW reference wind turbine for offshore system development," Nat. Renew. Energy Lab., Tech. Rep. NREL/TP-500-38060, 2009.

[40] W. Musial, S. Butterfield, and A. Boone, "Feasibility of floating platform systems for wind turbines," in *Proc. AIAA Aero. Sci. Mtg. and Exhibit*, 2004.

[41] M. Garcia-Sanz, "Control co-design: An engineering game changer," *Adv. Ctrl. Appl.*, 2019.

[42] K. P. Thiagarajan and H. J. Dagher, "A review of floating platform concepts for offshore wind energy generation," *J. Offshore Mech. and Arctic Eng.*, 2014.

[43] C. Bak, F. Zahle, R. Bitsche, T. Kim, A. Yde, L. C. Henriksen, A. Natarajan, and M. H. Hansen, "Description of the DTU-10MW reference wind turbine," DTU Wind Energy, Tech. Rep. I-0092, 2013.

[44] A. Robertson, J. Jonkman, M. Masciola, H. Song, A. Goupee, A. Coulling, and C. Luan, "Definition of the semisubmersible floating system for phase II of OC4," Nat. Renew. Energy Lab., Tech. Rep., 2014.

[45] W. Leithead and S. Dominguez, "Coordinated control design for wind turbine control systems," in *Proc. Euro. Wind Energy Conf.*, 2006.

[46] P. A. Fleming, I. Pineda, A. D. Wright, and D. Arora, "Evaluating methods for control of an offshore floating turbine," in *Proc. ASME Int. Conf. Ocean, Offshore and Arctic Eng.*, 2014.

[47] H. M. Johlas, L. A. Martinez-Tossas, M. J. Churchfield, M. A. Lackner, and D. P. Schmidt, "Floating platform effects on power generation in spar and semisubmersible wind turbines," *Wind Energy*, 2020.

[48] L. Ljung, *System Identification: Theory for the User*. Prentice Hall, 1999.

[49] H. K. Khalil, *Nonlinear Systems*. Prentice Hall, 1996.

[50] F. Lemmer, W. Yu, D. Schlipf, and P. W. Cheng, "Robust gain scheduling baseline controller for floating offshore wind turbines," *Wind Energy*, 2020.

[51] D. Stockhouse, M. Pusch, R. Damiani, S. Sirnivas, and L. Pao, "Robust multi-loop control of a floating offshore wind turbine," *Wind Energy*, 2023, under review.

[52] S. Skogestad and I. Postlethwaite, *Multivariable Feedback Control: Analysis and Design*. John Wiley & Sons, 2001.

[53] N. Abbas and L. Y. Pao, "On the controllability of a floating offshore wind turbine," *J. Phys.: Conf. Series*, 2020.

[54] E. Lenfest, A. J. Goupee, A. Wright, and N. Abbas, "Tuning of nacelle feedback gains for floating wind turbine controllers using a two-DOF model," in *Proc. ASME Int. Conf. Ocean, Offshore and Arctic Eng.*, 2020.

[55] B. Fischer and P. Loepelmann, "Balancing rotor speed regulation and drive train loads of floating wind turbines," *J. Phys.: Conf. Series*, 2016.

[56] T. Wakui, M. Yoshimura, and R. Yokoyama, "Multiple-feedback control of power output and platform pitching motion for a floating offshore wind turbine-generator system,"

Energy, 2017.
[57] G. Bir, "Multi-blade coordinate transformation and its application to wind turbine analysis," in *Proc. AIAA Aero. Sci. Mtg. and Exhibit*, 2008.
[58] E. A. Bossanyi, "Individual blade pitch control for load reduction," *Wind Energy*, 2003.
[59] H. Namik and K. Stol, "Disturbance accommodating control of floating offshore wind turbines," in *Proc. AIAA Aero. Sci. Mtg. and Exhibit*, 2009.
[60] S. Raach, D. Schlipf, F. Sandner, D. Matha, and P. W. Cheng, "Nonlinear model predictive control of floating wind turbines with individual pitch control," in *Proc. Amer. Ctrl. Conf.*, 2014.
[61] B. Xu, J. Feng, T. Wang, Y. Yuan, Z. Zhao, and W. Zong, "Trailing-edge flap control for mitigating rotor power fluctuations of a large-scale offshore floating wind turbine under the turbulent wind condition," *Entropy*, 2018.
[62] M. Zhang, X. Li, and J. Xu, "Smart control of fatigue loads on a floating wind turbine with a tension-leg-platform," *Renewable Energy*, 2019.
[63] L. Qi, H. Cao, Y. Zhang, M. Zhang, K. Shi, and J. Xu, "Data-driven control of the coupled loads for floating wind turbine systems based on deformable trailing edge flaps," *Ocean Eng.*, 2022.
[64] T. K. Barlas and G. A. van Kuik, "Review of state of the art in smart rotor control research for wind turbines," *Progress in Aerospace Sciences*, 2010.
[65] H. Lu, P. Zeng, L. Lei, Y. Yang, Y. Xu, and L. Qian, "A smart segmented blade system for reducing weight of the wind turbine rotor," *Energy Conversion and Management*, 2014.
[66] M. A. Lackner and M. A. Rotea, "Structural control of floating wind turbines," *Mechatronics*, 2011.
[67] D. Zalkind, M. Shields, E. Lenfest, A. Goupee, and C. Allen, "Open-loop control of adjustable tuned mass dampers for floating wind turbine platforms," in *Proc. Int. Ocean and Polar Eng. Conf.*, 2021.
[68] Z. Wu and Y. Li, "Platform stabilization of floating offshore wind turbines by artificial muscle based active mooring line force control," *IEEE/ASME Transactions on Mechatronics*, 2020.
[69] S. Park, M. A. Lackner, P. Pourazarm, A. R. Tsouroukdissian, and J. Cross-Whiter, "An investigation on the impacts of passive and semiactive structural control on a fixed bottom and a floating offshore wind turbine," *Wind Energy*, 2019.
[70] B. F. Spencer and S. Nagarajaiah, "State of the art of structural control," *J. Structural Eng.*, 2003.
[71] D. Roddier, C. Cermelli, A. Aubault, and A. Weinstein, "WindFloat: A floating foundation for offshore wind turbines," *J. Renewable Sustainable Energy*, 2010.
[72] A. Scholbrock, P. Fleming, D. Schlipf, A. Wright, K. Johnson, and N. Wang, "Lidar-enhanced wind turbine control: Past, present, and future," in *Proc. Amer. Ctrl. Conf.*, 2016.
[73] M. Harris, M. Hand, and A. Wright, "Lidar for Turbine Control," Nat. Renew. Energy Lab., Tech. Rep. NREL/TP-500-39154, 2005.
[74] D. Schlipf, E. Simley, F. Lemmer, L. Pao, and P. W. Cheng, "Collective pitch feedforward control of floating wind turbines using lidar," *J. Ocean and Wind Energy*, 2015.
[75] Y. Ma, P. D. Sclavounos, J. Cross-Whiter, and D. Arora, "Wave forecast and its application to the optimal control of offshore floating wind turbine for load mitigation," *Renewable Energy*, 2018.
[76] F. Lemmer, S. Raach, D. Schlipf, and P. W. Cheng, "Prospects of linear model predictive control on a 10 MW floating wind turbine," in *Amer. Soc. Mech. Eng. Dig. Collection*, Oct. 2015.
[77] K. A. Shah, Y. Li, R. Nagamune, Y. Zhou, and W. Ur Rehman, "Platform motion minimization using model predictive control of a floating offshore wind turbine," *Theoretical and Appl. Mech. Letters*, 2021.
[78] J. N. Newman, *Marine Hydrodynamics: 40th anniversary edition*. The MIT Press, 2017.
[79] E. Morris, H. Zienkiewicz, and M. Belmont, "Short-term forecasting of the sea-state," *Int. Shipbuilding Prog.*, 1998.
[80] A. Fontanella, M. Al, J.-W. van Wingerden, and M. Belloli, "Model-based design of a wave-feedforward control strategy in floating wind turbines," *Wind Energy Sci.*, 2021.
[81] J. Jonkman and M. Buhl, "FAST user's guide," Nat. Renew. Energy Lab., Tech. Rep., 2005.
[82] H. Namik and K. Stol, "Individual blade pitch control of floating offshore wind turbines," *Wind Energy*, 2009.
[83] D. Schlipf, F. Sandner, S. Raach, D. Matha, and P. W. Cheng, "Nonlinear model predictive control of floating wind turbines," in *Proc. Int. Offshore and Polar Eng.*, 2013.
[84] O. Bagherieh and R. Nagamune, "Gain-scheduling control of a floating offshore wind turbine above rated wind speed," *Ctrl. Theory & Tech.*, 2015.
[85] H. Suemoto, N. Hara, and K. Konishi, "Model-based design of individual blade pitch and generator torque controllers for floating offshore wind turbines," in *Proc. Asian Ctrl. Conf.*, 2017.
[86] N. Hara, S. Tsujimoto, Y. Nihei, K. Iijima, and K. Konishi, "Experimental validation of model-based blade pitch controller design for floating wind turbines: system identification approach," *Wind Energy*, 2017.
[87] T. Bakka, H.-R. Karimi, and S. Christiansen, "Linear parameter-varying modelling and control of an offshore wind turbine with constrained information," *IET Ctrl. Theory & Appl.*, 2014.
[88] F. Thiery, N. Hara, and K. Konishi, "Model predictive control for floating offshore wind turbines with failure compensation using individual blade pitch control," in *Int. Conf. Ctrl., Automation, and Sys.*, 2015.
[89] E. Lindeberg, H. G. Svendsen, and K. Uhlen, "Smooth transition between controllers for floating wind turbines," *Energy Procedia*, 2012.
[90] B. Shahsavari, O. Bagherieh, N. Mehr, R. Horowitz, and C. Tomlin, "Optimal mode-switching and control synthesis for floating offshore wind turbines," in *Proc. Amer. Ctrl. Conf.*, 2016.
[91] T. Wakui, A. Nagamura, and R. Yokoyama, "Stabilization of power output and platform motion of a floating offshore wind turbine-generator system using model predictive control based on previewed disturbances," *Renewable Energy*, 2021.
[92] L. Pustina, F. Biral, and J. Serafini, "A novel nonlinear model predictive controller for power maximization on floating offshore wind turbines," *J. Phys.: Conf. Series*, 2022.
[93] Y. Okada, K. Haneda, T. Chujo, and T. Ohtsuka, "Parameter-varying modeling and nonlinear model predictive control with disturbance prediction for spar-type floating offshore wind turbines," *J. Marine Sci. & Tech.*, Mar. 2022.
[94] T. Casey, "World's biggest floating offshore wind farm is powering oil & gas platforms in the North Sea," https://cleantechnica.com/2022/11/22/worlds-biggest-floating-offshore-wind-farm-is-powering-oil-gas-platforms-in-the-north-sea/, 2022, accessed Jan. 2023.
[95] S. Boersma, B. M. Doekemeijer, P. M. Gebraad, P. A. Fleming, J. Annoni, A. K. Scholbrock, J. A. Frederik, and J.-W. van Wingerden, "A tutorial on control-oriented modeling and control of wind farms," in *Proc. Amer. Ctrl. Conf.*, 2017.
[96] S. Emeis, S. Siedersleben, A. Lampert, A. Platis, J. Bange, B. Djath, J. Schulz-Stellenfleth, and T. Neumann, "Exploring the wakes of large offshore wind farms," *J. Phys.: Conf. Series*, 2016.
[97] L. A. Martínez-Tossas, J. King, E. Quon, C. J. Bay,

R. Mudafort, N. Hamilton, M. F. Howland, and P. A. Fleming, "The curled wake model: a three-dimensional and extremely fast steady-state wake solver for wind plant flows," *Wind Energy Sci.*, 2021.

[98] A. S. Wise and E. E. Bachynski, "Wake meandering effects on floating wind turbines," *Wind Energy*, 2020.

[99] S. Rockel, E. Camp, J. Schmidt, J. Peinke, R. B. Cal, and M. Hölling, "Experimental study on influence of pitch motion on the wake of a floating wind turbine model," *Energies*, 2014.

[100] A. C. Kheirabadi and R. Nagamune, "A low-fidelity dynamic wind farm model for simulating time-varying wind conditions and floating platform motion," *Ocean Eng.*, 2021.

[101] W. Munters and J. Meyers, "Towards practical dynamic induction control of wind farms: analysis of optimally controlled wind-farm boundary layers and sinusoidal induction control of first-row turbines," *Wind Energy Sci.*, 2018.

[102] J. A. Frederik, B. M. Doekemeijer, S. P. Mulders, and J.-W. van Wingerden, "The helix approach: Using dynamic individual pitch control to enhance wake mixing in wind farms," *Wind Energy*, 2020.

[103] G. Froese, S. Y. Ku, A. C. Kheirabadi, and R. Nagamune, "Optimal layout design of floating offshore wind farms," *Renewable Energy*, 2022.

[104] A. C. Kheirabadi and R. Nagamune, "Real-time relocation of floating offshore wind turbines for power maximization using distributed economic model predictive control," in *Proc. Amer. Ctrl. Conf.*, 2021.

[105] C. Han and R. Nagamune, "Platform position control of floating wind turbines using aerodynamic force," *Renewable Energy*, 2020.

[106] M. Vali, V. Petrović, L. Y. Pao, and M. Kühn, "Model predictive active power control for optimal structural load equalization in waked wind farms," *IEEE Trans. Ctrl. Sys. Tech.*, 2022.

[107] M. Vali, V. Petrović, S. Boersma, J.-W. van Wingerden, L. Y. Pao, and M. Kühn, "Adjoint-based model predictive control for optimal energy extraction in waked wind farms," *Ctrl. Eng. Practice*, 2019.

[108] M. M. Montero, V. Arcari, S. Cacciola, and A. Croce, "Effectiveness of dynamic induction control strategies on the wake of a wind turbine," *J. Phys.: Conf. Series*, 2022.

[109] A. C. Kheirabadi and R. Nagamune, "Real-time relocation of floating offshore wind turbine platforms for wind farm efficiency maximization: An assessment of feasibility and steady-state potential," *Ocean Eng.*, 2020.

[110] Nat. Renew. Energy Lab., "OpenFAST," Software, 2021. [Online]. Available: https://github.com/OpenFAST/openfast

[111] T. J. Larsen and A. M. Hansen, *How 2 HAWC2, the user's manual*. Risø Nat. Lab., 2007.

[112] J. Rinker, E. Gaertner, F. Zahle, W. Skrzypiński, N. Abbas, H. Bredmose, G. Barter, and K. Dykes, "Comparison of loads from HAWC2 and OpenFAST for the IEA Wind 15 MW reference wind turbine," *J. Phys.: Conf. Series*, 2020.

[113] DNV-GL, "Bladed," 2018. [Online]. Available: https://www.dnvgl.com/energy

[114] Orcina, "OrcaFlex," Software, 2022. [Online]. Available: https://www.orcina.com/orcaflex/

[115] M. Hall, S. Housner, D. Ogden, D. Zalkind, G. Barter, and P. Bortolotti, "RAFT (Response Amplitudes of Floating Turbines)," Nat. Renew. Energy Lab., Tech. Rep., 2022.

[116] F. Lemmer, W. Yu, B. Luhmann, D. Schlipf, and P. W. Cheng, "Multibody modeling for concept-level floating offshore wind turbine design," *Multibody Sys. Dyn.*, 2020.

[117] M. H. Hansen and L. C. Henriksen, "Basic DTU Wind Energy controller," Tech. Univ. Denmark, Tech. Rep. E-0018, 2013.

[118] N. Abbas, "Enabling automated control co-design for wind turbines," Ph.D. dissertation, Univ. Colorado Boulder, 2022.

[119] NREL, "FLORIS version 3.1," 2022. [Online]. Available: https://github.com/NREL/floris

[120] Y. Niu, P. Lathi, and R. Nagamune, "Floating offshore wind farm control via turbine repositioning with aerodynamic force," *Proc. Amer. Ctrl. Conf.*, 2023.

[121] J. Jonkman and K. Shaler, "FAST.Farm user's guide and theory manual," Nat. Renew. Energy Lab., Tech. Rep., 2021.

[122] F. Madsen, T. Nielsen, T. Kim, H. Bredmose, A. Pegalajar-Jurado, R. Mikkelsen, A. Lomholt, M. Borg, M. Mirzaei, and P. Shin, "Experimental analysis of the scaled DTU10MW TLP floating wind turbine with different control strategies," *Renewable Energy*, 2020.

[123] H. Bredmose, F. Lemmer, M. Borg, A. Pegalajar-Jurado, R. F. Mikkelsen, T. S. Larsen, T. Fjelstrup, W. Yu, A. K. Lomholt, L. Boehm, and J. A. Armendariz, "The triple spar campaign: Model tests of a 10MW floating wind turbine with waves, wind and pitch control," *Energy Procedia*, 2017.

[124] H. Kakuya, T. Shiraishi, S. Yoshida, T. Utsunomiya, and I. Sato, "Experimental results of floating platform vibration control with mode change function using full-scale spar-type floating offshore wind turbine," *Wind Eng.*, 2018.

[125] H. Kakuya, S. Yoshida, I. Sato, and T. Utsunomiya, "Proposal for a lower limit control of a generator's torque based on the nacelle wind speed and demonstration results using a full-scale spar-type floating offshore wind turbine," *Wind Eng.*, 2020.

[126] A. Otter, J. Murphy, V. Pakrashi, A. Robertson, and C. Desmond, "A review of modelling techniques for floating offshore wind turbines," *Wind Energy*, 2022.

[127] "ARPA-E ATLANTIS program," https://arpa-e.energy.gov/technologies/programs/atlantis, 2019, accessed Jan. 2023.

[128] R. Kimball, A. Robertson, M. Fowler, N. Mendoza, A. Wright, A. Goupee, E. Lenfest, and A. Parker, "Results from the FOCAL experiment campaign 1: turbine control co-design," *J. Phys.: Conf. Series*, 2022.

[129] J. Manwell, J. McGowan, and A. Rogers, *Wind Energy Explained: Theory, Design, and Application*. Wiley, 2010.

[130] E. Mollerstrom, P. Gipe, J. Beurskens, and F. Ottermo, "A historical review of vertical axis wind turbines rated 100 kW and above," *Renew. & Sustainable Energy Rev.*, 2019.

[131] M. Borg, A. Shires, and M. Collu, "Offshore floating vertical axis wind turbines, dynamics modelling state of the art. Part I: Aerodynamics," *Renew. & Sustainable Energy Rev.*, 2014.

[132] D. T. Griffith, J. P. M. Barone, B. Owens, D. Bull, C. Simao-Ferriera, A. Goupee, and M. Fowler, "Design studies for deep-water floating offshore vertical axis wind turbines," Sandia Nat. Lab., Tech. Rep. SAND2018-7002, 2018.

[133] A. Arredondo-Galeana and F. Brennan, "Floating offshore vertical axis wind turbines: Opportunities, challenges and way forward," *energies*, 2021.

[134] T. Stehly and P. Duffy, "2020 cost of wind energy review," Nat. Renew. Energy Lab., Tech. Rep. NREL/TP-5000-81209, 2022.

[135] ABS Group, "Floating offshore wind turbine development assessment," Bureau of Ocean Energy Management, Tech. Rep. BOEM 2021-030, 2021.

[136] S. Bashetty and S. Ozcelik, "Design and stability analysis of an offshore floating multi-wind turbine platform," *Inventions*, 2022.

[137] https://cleantechnica.com/2022/06/17/gm-falls-for-crazy-floating-wind-turbine-idea-may-not-be-so-crazy-after-all/, 2022, accessed Oct. 2022.